Creep modulation of Omori law generated by a Coulomb stress perturbation in a 3-D rate-and-state asperity model

Pierre Dublanchet, Pascal Bernard, P. Favreau

JOURNAL OF GEOPHYSICAL RESEARCH: SOLID EARTH, VOL. 118, 4774–4793, doi:10.1002/jgrb.50311, 2013

Creep modulation of Omori law generated by a Coulomb stress perturbation in a 3-D rate-and-state asperity model

P. Dublanchet,[1] P. Bernard,[1] and P. Favreau[1]

Received 11 April 2013; revised 25 July 2013; accepted 27 July 2013; published 9 September 2013.

[1] We present numerical simulations conducted with a quasi-dynamic, 3-D rate-and-state asperity model and an analytical approach in order to study the behavior of a seismic asperity surrounded by aseismic creep in response to external Coulomb stress perturbations. This work is inspired by the observation of Omori decay characterizing the recurrence time of isolated repeating earthquakes, such as at the Parkfield segment of the San Andreas Fault during the postseismic phase of the 2004 M_W6 event. Based on the numerical results and on an analysis of phase diagrams, we identify two possible regimes that characterize the response of an asperity surrounded by aseismic creep to a stress step, depending on an effective steady state friction parameter A. For the specific perturbation used in this study, we observe that when A is positive, the relaxation of the system is governed by the response of the creeping segments of the fault, and the asperity ruptures in an Omori sequence. In this regime, we demonstrate that the duration of the relaxation process depends on A. Furthermore, we show that this effective strengthening behavior is equivalent to a subcritical density of asperities meaning that the shape of the Omori decay is controlled by the relative proportion of seismic and aseismic material within the fault. On the other hand, a fault characterized by effective steady state weakening ($A < 0$) behaves like a spring and slider system that loses the memory of the stress perturbation once the first aftershock occurred, at least in the simulations presented here.

Citation: Dublanchet, P., P. Bernard, and P. Favreau (2013), Creep modulation of Omori law generated by a Coulomb stress perturbation in a 3-D rate-and-state asperity model, *J. Geophys. Res. Solid Earth*, *118*, 4774–4793, doi:10.1002/jgrb.50311.

1. Introduction

[2] Observations of aftershock activity related to major earthquake revealed the high correlation between stressed areas and enhanced activity regions [*King et al*., 1994; *Harris*, 1998; *Harris and Simpson*, 1998; *Toda et al*., 1998; *Stein*, 1999; *Toda et al*., 2005; *Stein et al*., 2007]. In addition to the instantaneous response of seismic activity to a stress change in the crust, the decay of seismicity rate has also been widely analyzed and is well characterized by a power law, first established by *Omori* [1894] [see also *Utsu et al.*, 1995], and usually called Omori law.

[3] Even if these properties of triggered seismicity are now well accepted, physical models supporting these observations remain limited. One of the most popular attempts to model seismicity in response to stress perturbations is the work of *Dieterich* [1994] taking into account the laboratory-derived rate-and-state friction law [*Dieterich*, 1979]. In his model, the Omori decay is a consequence of the time dependence of the nucleation process controlled by rate-and-state friction. This model has been further extended in several works, including the numerical approaches of *Gomberg et al*. [1998, 2000, 2005] and *Belardinelli et al.* [2003] and the models of *Perfettini et al.* [2003] and *Kaneko and Lapusta* [2008] who studied the effect of stress perturbations on the time to failure of one-dimensional rate-and-state faults embedded in two-dimensional elastic media with various friction properties and initial conditions, improving in this manner the description of nucleation.

[4] However, all the models previously mentioned do not take into consideration the possibility of fault creep, especially in the case of postseismic afterslip, and its forcing on postseismic activity. Several authors indeed provided direct evidences of aseismic creep forcing aftershock activity: *Schaff et al.* [1998] in their study of Loma Prieta aftershocks, *Lengliné et al.* [2009] in the case of Parkfield repeaters, and *Bourouis and Bernard* [2007] in their analysis of the seismicity triggered by a fluid injection at 3 km depth in Soultz-sous-Fort (France). In these latter studies, the authors identified repeating isolated earthquakes, and showed how recurrence time of these events changes in response to a nearby main shock, leading to an Omori decay of seismicity, at the scale of a single repeater. From this kind of observations emerges a possible mechanical model for aftershock sequences driven by aseismic slip, in which

Companion to *Dublanchet et al.* [2013], doi:10.1002/jgrb.50187.

[1]Laboratoire de sismologie, Institut de Physique du Globe de Paris, Paris, France.

Corresponding author: P. Dublanchet, Institut de Physique du Globe de Paris, 1 rue Jussieu, FR-75238 Paris CEDEX 05, France. (dublanchet@ipgp.fr)

2169-9313/13/10.1002/jgrb.50311

aftershock sequences would be generated by the rupture of asperities distributed on a creeping fault and suddenly forced by the acceleration of the aseismic deformation caused by the main event.

[5] These processes of interaction between creep and seismic asperities have been recently studied by *Kato* [2007], *Ziv* [2007], *Helmstetter and Shaw* [2009], *Ariyoshi et al.* [2009, 2012], *Kaneko et al.* [2010], *Ader et al.* [2012], *Skarbek et al.* [2012], and *Dublanchet et al.* [2013], and in all these attempts, it has been proposed that the different regimes of behavior of such systems of asperities surrounded by creep could be separated in terms of density of asperities. In other words, a creeping fault containing seismic asperities could produce aseismic slip and tremors, as well as independent or highly clustered seismicity depending on the relative proportion of creeping and seismic fault material. Furthermore, *Dublanchet et al.* [2013] showed that the existence of strong interactions among a population of sources is only possible for a density of asperities that exceeds a critical threshold. In this framework, the Omori decay observed by *Schaff et al.* [1998], *Bourouis and Bernard* [2007], and *Lengliné et al.* [2009] might also be controlled by the density of asperities characterizing the fault.

[6] Motivated by the work of *Schaff et al.* [1998], *Bourouis and Bernard* [2007], and *Lengliné et al.* [2009], we consider here a single repeater isolated on a creeping fault, and we propose in the following study to address the question of how the shape of the Omori law generated by a creep transient on a planar fault hosting a single seismic asperity could be controlled by the ratio between area occupied by the asperity and aseismic area, which is equivalent to the density of asperities defined by *Dublanchet et al.* [2013]. In order to address this issue, we adopted the 3-D mechanical approach developed by *Dublanchet et al.* [2013] which enables to compute the stress and slip evolution of a seismic asperity embedded in a creeping fault in response to various stressing histories. Our attempt thus generalizes the study of *Ziv* [2007] who assumed a similar system of an isolated asperity embedded in a creeping fault and perturbed by a coseismic stress step. *Ziv* [2007] indeed only analyzed a specific density of asperities and did not investigate the influence of the amount of creeping material on the fault in the response to a stress perturbation. Furthermore, our 3-D model overcomes the limitations of the 2-D approach used by *Ziv* [2007] and allows to consider realistic geometries of sources as inferred from multiplet observations. Moreover, the use of a 2-D heterogeneous fault (with an asperity surrounded by creep) extends the attempt of *Perfettini and Ampuero* [2008] who studied the response of a uniformly velocity strengthening fault to a particular shear stress perturbation of Gaussian shape without taking into account the interaction between aseismic creep and seismic sources. To this point, we emphasize that we adopt a slightly different point of view than what has been done by *Perfettini et al.* [2003] and *Kaneko and Lapusta* [2008] with similar numerical models, in the sense that we are not interested in the timing of the first rupture of the system, but we rather study the long-term evolution of the fault after a stress perturbation, that is, at a longer timescale than the first seismic event.

[7] In the following, we first describe the numerical model (constitutive equations, fault geometry, and loading conditions). In particular, we introduce the concept of density of asperities. After briefly discussing the unperturbed evolution of the system, we present the method used to impose stress steps, and we analyze in detail two opposite examples of perturbations. These first results will allow us to identify the density of asperities as the relevant parameter controlling the relaxation process that occurs on the fault in response to a stress perturbation. In a second step, we derive an analytical model based on the analysis of phase diagrams and average stress, which leads to an expression of the timescale of the relaxation of the fault in terms of density of asperities. Finally, we apply the new theoretical concepts developed here to the case of the Parkfield repeaters analyzed by *Lengliné et al.* [2009], and we provide an interpretation of the Omori law observed at the scale of a single asperity in terms of the ratio between seismic source dimension and surrounding aseismic area dimension.

2. Model Formulation

2.1. Fault System and Boundary Conditions

[8] In the following sections, we consider the periodic system presented in Figure 1, consisting of the repetition of a planar fault S with one single circular asperity surrounded by aseismic creep separating two homogeneous elastic half spaces ($z > 0$ and $z < 0$). The use of periodic boundary conditions for the fault segment S of interest allows the use of efficient fast Fourier transform (FFT) technics in the numerical resolution of the equations governing the evolution of slip on S as this has been mentioned by *Dublanchet et al.* [2013]. The resulting infinite regular distribution of asperities is unrealistic and it would be more appropriate to model natural fault segments with a single asperity surrounded by a creeping region bounded by either locked or freely sliding fault environment. However, as this will be detailed in the discussion section, the periodic distribution could locally be considered as an equivalent model for the freely slipping boundary case, as long as the asperities are enough scattered so that they do not interact with each other. More generally, the purpose of this study is to investigate the effective response of a heterogeneous fault to a stress perturbation, rather than reproducing the behavior of a particular repeating earthquake perturbed by a nearby main shock, and as it will be shown in the following, the simplified periodic geometry used here allows to capture the most important physical processes underlying the response of heterogeneous faults. The fault plane is divided into n_x by n_y computational cells and is loaded at a constant rate v_p in the x direction at a distance $w/2$ in the fault normal direction.

2.2. Rate-and-State Friction: Modeling Asperities and Fault Creep

[9] The frictional shear stress $\tau(\mathbf{x}, t)$ in the x direction at point $\mathbf{x}$ and time t on the fault plane obeys rate-and-state law [*Dieterich*, 1979; *Rice*, 1983] and is expressed as

$$\tau(\mathbf{x}, t) = \sigma(\mathbf{x}, t)\left[\mu_0 + a(\mathbf{x}) \ln \frac{v(\mathbf{x}, t)}{v_p} + b(\mathbf{x})\Theta(\mathbf{x}, t)\right], \qquad (1)$$

where σ is the normal stress, μ_0 is a reference coefficient of friction, v_p is the tectonic loading rate imposed at $z = w/2$, $a(\mathbf{x})$ and $b(\mathbf{x})$ are nondimensional parameters, $v(\mathbf{x}, t)$ is the sliding velocity, and $\Theta(\mathbf{x}, t)$ is the state variable that evolves

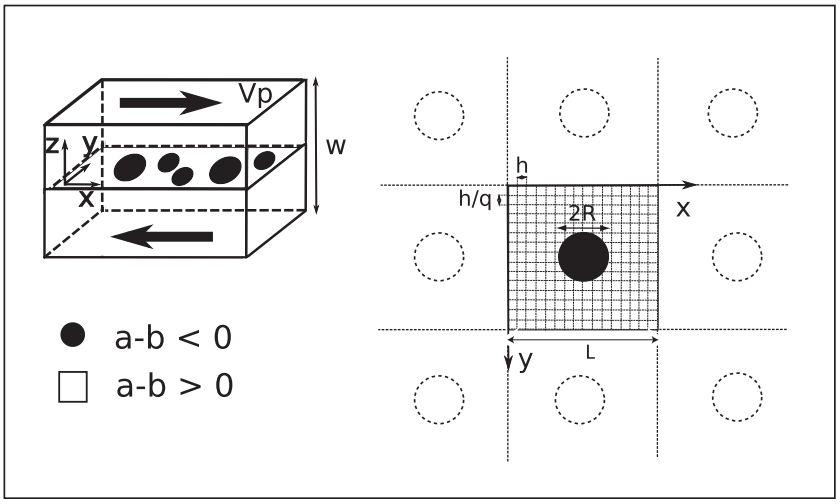

Figure 1. (left) Schematic block diagram showing the planar fault separating two elastic blocks of thickness $w/2$. The large black arrows indicate the direction of shear loading rate imposed on each opposite side of the system. Black patches on the fault represent asperities with velocity weakening friction properties ($a-b<0$) surrounded by velocity strengthening properties ($a-b>0$). (right) Fault plane geometry assumed in this study, with the main fault S represented by solid lines and its repetitions along x and y axes. The computational grid made of square cells h/q by h is also shown as well as a single circular asperity of radius R. L is the size of the main fault.

with slip history and normal stress. This latter dependence is taken into account by specifying an evolution law for Θ. For that, we follow *Ruina* [1983] and *Linker and Dieterich* [1992], and we choose to work with the slip formulation of the state evolution law:

$$\dot{\Theta}(\mathbf{x},t) = -\frac{v(\mathbf{x},t)}{d_c}\left[\Theta(\mathbf{x},t) + \ln\frac{v(\mathbf{x},t)}{v_p}\right] - \frac{\alpha\dot{\sigma}(\mathbf{x},t)}{b(\mathbf{x})\sigma(\mathbf{x},t)}, \qquad (2)$$

where d_c is a characteristic length, usually interpreted as the slip necessary to renew a population of microscopic contacts, $b(\mathbf{x})$ is the friction parameter defined in (1), and α is a constant parameter introduced by *Linker and Dieterich* [1992] that quantifies the instantaneous effect of a normal stress step on the state variable, as will be shown later. If $\dot{\Theta}=0$ and $\dot{\sigma}=0$, the system is at steady state, and the corresponding frictional strength $\tau_{ss}(\mathbf{x},t)$ depends only on sliding velocity in the following way:

$$\tau_{ss}(\mathbf{x},t) = \sigma(\mathbf{x},t)\left[\mu_0 + (a-b)(\mathbf{x})\ln\frac{v(\mathbf{x},t)}{v_p}\right]. \qquad (3)$$

Two distinct steady state behaviors emerge from expression (3) depending on the sign of $(a-b)$ parameter: either velocity weakening if $(a-b)<0$ or velocity strengthening if $(a-b)>0$. We will next define the asperity on the fault plane by assigning velocity weakening friction properties to the circular patch large enough to be seismically destabilized, as was previously done by *Kato* [2003, 2004], *Chen and Lapusta* [2009], and *Dublanchet et al.* [2013]. The critical minimum radius of the patches allowing the occurrence of seismic events was determined empirically for our simulations. In order to allow the possibility of aseismic slip in the surroundings of the asperity, we assign velocity strengthening friction properties to the other portions of the fault plane. This distribution of frictional properties is represented in Figure 1. An important requirement of our modeling procedure is that the process zone is well resolved. For the values of friction parameters a and b considered in this study, *Ampuero and Rubin* [2008a] showed that this condition is satisfied in 2-D models of faults obeying rate-and-state friction with the slip law for the state evolution, as long as the cell size h is smaller than the length scale $L_{b'}$ defined by

$$L_b' = \frac{L_b}{\ln(v_m/v_p)} = \frac{Gd_c}{b\sigma\ln(v_m/v_p)}, \qquad (4)$$

where b is estimated on the asperity, G is the shear modulus of the medium, and v_m is the maximum sliding velocity on the asperity during the rupture process. In our simulations, the maximum sliding velocity is on the order of 1 m s^{-1}, leading to values of $\ln(v_m/v_p)$ of the order of 20. Therefore, we used a computational cell size smaller than $0.05L_b$. In this sense, our model is continuous and allows for a rather correct description of nucleation on the process zone. Since the scaling given by equation (4) is not exact, we present in Appendix A resolution tests conducted to determine the maximum cell size allowed in our problem.

2.3. Quasi-Dynamic Elastic Interactions

[10] On the fault plane considered, the frictional resistance is balanced by elastic interactions. In order to model the static component of these interactions, we adopt the same elastic kernel as *Dublanchet et al.* [2013] and derived by *Maruyama* [1964]. Furthermore, we approximate the local dynamic effects on the fault by adding to the static term a radiation damping term, first introduced by *Rice* [1993], that roughly estimates the stress change on a point of the fault due to slip on this point by accounting for the stress induced by elastic waves radiated in the fault-normal

Table 1. List of Parameters

Parameters	Value
Asperity a parameter a_w	0.001
Asperity b parameter b_w	0.005
Antiasperity a parameter a_s	0.005
Antiasperity b parameter b_s	0.001
α parameter	0.2
Critical slip d_c	0.2 mm
Loading rate v_p	10^{-9} m s^{-1} = 3.15 cm yr^{-1}
Shear modulus G	30 GPa
Shear wave speed β	3 km s^{-1}
Thickness of the medium w	3 km
Fault length L	72 m/192 m
Unperturbed normal stress σ_0	100 MPa
Radiation damping η	5.10^6 Pa s m^{-1}
Computational cell y dimension h	0.375 m
Computational cell aspect ratio q	1
h/L_b	0.03
Radius of asperity R	30 m

direction. The shear stress τ_e on a point $\mathbf{x}$ of the fault S is therefore expressed in the following way:

$$\tau_e(\mathbf{x},t) = \tau^* - \frac{G}{w}\left[\delta(\mathbf{x},t) - v_p t\right] + \int_S \kappa(\mathbf{x}-\mathbf{x_0})\left[\delta(\mathbf{x_0},t) - v_p t\right] \mathrm{d}\mathbf{x_0} - \eta\left[v(\mathbf{x},t) - v_p\right] + \Delta\tau(\mathbf{x},t), \quad (5)$$

where τ^* is a reference value of stress and $\kappa(\mathbf{x}-\mathbf{x_0})$ is the periodic elastic kernel derived from *Kato* [2003] and *Maruyama* [1964], giving stress on point $\mathbf{x}$ caused by displacement δ on point $\mathbf{x_0}$ of S, and on all the periodic replicas of $\mathbf{x_0}$ (see Figure 1). The use of such an elastic kernel that is computed for an elastic half-space introduces some error in the estimation of the elastic interactions in our finite geometry (imposed velocity boundary condition at $w/2$; Figure 1). However, according to *Dublanchet et al.* [2013], this error is negligible as long as $w/2$ is much larger than the size of the fault L as this is the case here (see Table 1). The second term on the right-hand side of equation (5) is the loading contribution to shear stress associated with imposed motion at a distance $w/2$ in the fault normal direction. The third term represents the planar static interactions, and the fourth one is the radiation damping term, η being the damping coefficient of *Rice* [1993] defined as the ratio between shear modulus G and 2 times the shear wave speed β. Finally, the last term represents shear stress loading perturbations imposed on the system.

2.4. Computational Method

[11] In this study, we compute the stress and velocity evolution on each point of the fault plane using the method developed by *Dublanchet et al.* [2013] which involves an adaptive time step Runge-Kutta algorithm [*Press et al.*, 2007] and a computation of elastic interactions through FFT technics developed by *Swarztrauber* [1982] and *Swarztrauber* [1984].

2.5. Model Parameters

[12] In the following section, we focus on the problem of the evolution of a single circular asperity of radius R embedded in a creeping fault and its response to different stress steps (normal and shear steps). Furthermore, we exclusively considered homogeneous perturbations over the entire fault plane, so that normal stress does not depend on $\mathbf{x}$. This last point implies that we also neglect variations of normal stress along the fault that would exist in the case of a dipping or vertical fault plane. Nevertheless, because of the small size of the fault considered here, the lithostatic normal stress variation should not exceed 5% between two distant points of the fault. In the next sections, we will refer to the creeping, velocity strengthening surroundings of the asperity as antiasperity, characterized by friction parameters a_s and b_s, while the asperity is characterized by a_w and b_w. Furthermore, according to *Dublanchet et al.* [2013], we define the density of asperities ρ by the ratio between velocity weakening area and velocity strengthening area that could be written, in the case of a single asperity of radius R, as

$$\rho = \frac{\pi R^2}{L^2}, \quad (6)$$

with L being the size of the fault plane considered, as indicated in Figure 1. In order to get different values of ρ, we chose to work at constant R and to use different values of L.

[13] The values of the different parameters used in this study are summarized in Table (1). For friction parameter values, we mainly used the work of *Marone* [1998] and tried to use a value of $(b-a)_w$ that leads to reasonable stress drop on the asperity. With our choice, the mean stress drop during a seismic event is around 7 MPa, which is in the range of what is inferred for Parkfield asperities by *Nadeau and Johnson* [1998] and *Dreger et al.* [2007]. In order to reduce the computational cost of our simulations, we used a ratio a_w/b_w of 0.2 on the asperity, which is to some extent an underestimation of the experimental values usually reported [*Kilgore et al.*, 1993; *Blanpied et al.*, 1998] that are of the order of 0.8 or 0.9. According to *Ampuero and Rubin* [2008a], a larger ratio a_w/b_w would modify the acceleration of slip on the asperity during nucleation. More generally, the shape of the seismic cycle on the asperity could be modified, as well as the amount of aseismic deformation on the asperity itself and the total duration of the unperturbed seismic cycle, even if the stress drop remains the same. However, this study focuses on the relative change in the rhythm of ruptures affecting the asperity, without considering the unperturbed duration of the seismic cycle. Furthermore, we will only analyze in the following a relaxation process that is mostly controlled by the strengthening parts of the system and independent of the shape of the seismic cycle.

[14] The background normal stress σ used in this study could either represent the value of the effective normal stress in the case of an overpressurized fault according to *Rice* [1992], or in the absence of such over-pressurized fluids, to the lithostatic pressure expected at around 3 km depth, assuming a shear wave speed of 3 km s^{-1} and a rigidity of 30 GPa. In the latter situation, σ = 100 MPa could be the approximate normal stress experienced by the most superficial repeaters in Parkfield relocated by *Lengliné et al.* [2009]. The loading rate v_p is also in the range of the creep rate measured at Parkfield by *Murray et al.* [2001] and *Titus et al.* [2006]. Note that the loading rate is imposed at a distance more than three times larger than the dimension of the fault plane, so that this term does not perturb the elastic interactions in the fault plane but allows for rapid convergence of

Table 2. List of Simulations[a]

n^0	a_s	b_s	a_s/b_s	ρ	Percent Cycle	Δcff (MPa)	ρ/ρ_c	ρ/ρ_c^*
1	5.10^{-3}	10^{-3}	5	0.4	60 %	0.8	0.85	0.9
2	5.10^{-3}	10^{-3}	5	0.35	60 %	0.8	0.7	0.75
3	5.10^{-3}	10^{-3}	5	0.3	60 %	0.8	0.65	0.65
4	5.10^{-3}	10^{-3}	5	0.25	60 %	0.8	0.5	0.55
5	5.10^{-3}	10^{-3}	5	0.2	60 %	0.8	0.4	0.45
6	5.10^{-3}	10^{-3}	5	0.15	60 %	0.8	0.3	0.35
7	5.10^{-3}	2.10^{-3}	2.5	0.3	60 %	0.8	0.75	0.8
8	4.10^{-3}	10^{-3}	4	0.3	60 %	0.8	0.75	0.8
9	5.10^{-3}	3.10^{-3}	1.66	0.3	60 %	0.8	0.95	1.05
10	3.10^{-3}	10^{-3}	3	0.3	60 %	0.8	0.95	1.1
11	5.10^{-3}	10^{-3}	5	0.4	30 %	–0.8	0.85	0.9
12	5.10^{-3}	10^{-3}	5	0.35	30 %	–0.8	0.7	0.75
13	5.10^{-3}	10^{-3}	5	0.3	30 %	–0.8	0.65	0.65
14	5.10^{-3}	10^{-3}	5	0.25	30 %	–0.8	0.5	0.55
15	5.10^{-3}	10^{-3}	5	0.2	30 %	–0.8	0.4	0.45
16	5.10^{-3}	10^{-3}	5	0.55	60 %	0.8	1.15	1.2
17	5.10^{-3}	10^{-3}	5	0.55	30 %	–0.8	1.15	1.2

[a] ρ_c and ρ_c^* are computed from equations (9) and (28), respectively, assuming a stress drop $\Delta\tau_0$ = 7 MPa, and v_{sis} = 1 cm s^{-1}.

the system toward a limit cycle in which the system follows the loading rate.

2.6. Stress Perturbations

[15] In the next sections, we analyze the effect of instantaneous steps of shear and normal stress on the evolution of a single circular asperity centered on the creeping fault. The system initially characterized by $(\tau_0, \sigma_0, v_0, \Theta_0)$ will instantaneously evolve toward $(\tau_1, \sigma_1, v_1, \Theta_1)$ at the onset of the stress perturbation. In the following, we will use the instantaneous changes of the variables defined as $\tau_1 - \tau_0 = \Delta\tau$, $\sigma_1 - \sigma_0 = \Delta\sigma$, $\Theta_1 - \Theta_0 = \Delta\Theta$, and $v_1 - v_0 = \Delta v$. Since our numerical model is based on the resolution of the equations of evolution for sliding velocity v and state variable Θ, and not directly on the evaluation of stress that is deduced a posteriori from the rate-and-state friction law (1), we have to define the effect of shear and normal stress changes $\Delta\tau$ and $\Delta\sigma$ on the state variable and on the sliding velocity. Following *Linker and Dieterich* [1992] and *Perfettini et al.* [2003], we define v_1 and Θ_1 as

$$\Theta_1 = \Theta_0 - \frac{\alpha}{b} \ln\left(1 + \frac{\Delta\sigma}{\sigma_0}\right), \tag{7}$$

$$v_1 = v_0 \left(1 + \frac{\Delta\sigma}{\sigma_0}\right)^{\alpha/a} \exp\left[\frac{\Delta cff(\mu)}{a\sigma_1}\right], \tag{8}$$

where b is the state parameter of the rate-and-state friction law (1) and α is the parameter linking normal stress variation to state variations in formula (2). Furthermore, we have introduced the Coulomb stress change defined by *Perfettini et al.* [2003] as $\Delta cff(\mu) = \Delta\tau - \mu(v_0, \Theta_0)\Delta\sigma$, with $\mu(v_0, \Theta_0)$ being the friction coefficient on the fault at the onset of the stress step.

3. Numerical Experiments

[16] In order to study the postseismic response of the asperity surrounded by creep previously described, we conducted a series of simulations described in Table 2. We limited our study to spatially uniform Coulomb stress perturbations. The underlying assumption of doing so is that the system made of the asperity and its creeping surroundings is much smaller than the main shock at the origin of the stress perturbation, which seems reasonable if the difference in the magnitudes between the main shock and the aftershock is large enough.

[17] Note that in every simulations, the stress perturbation occurs either at 60% or at 30% of the seismic cycle of the asperity. As mentioned by *Ziv* [2007], the postseismic activity of the asperity strongly depends on the timing of the coseismic stress step within the seismic cycle of the asperity, because of the evolution of the initial conditions on the fault at the onset of the perturbation. For that reason, we will only draw comparisons between systems that experienced the stress step in the same conditions, which means that we will discuss separately the results obtained in the simulations labeled 60% and 30% in Table 2.

[18] Furthermore, as shown in Table 2, we will focus on two particular Coulomb stress perturbations. The first one consists in a positive shear stress step of amplitude $\Delta\tau$ = 0.8 MPa at constant normal stress, whereas the second perturbation corresponds to a positive normal stress perturbation $\Delta\sigma$ = 1.3 MPa at constant shear stress. In each case, the Coulomb stress perturbation is of similar magnitude, but of opposite sign, as long as μ is approximately equal to μ_0. As demonstrated by *Perfettini et al.* [2003], this latter assumption is reasonable for most of the seismic cycle, and it only fails in the last part of the interseismic period when the instability is nucleating. In particular, this assumption is acceptable at 30% and 60% of the interseismic period when the perturbation starts in our simulations. We chose these two cases because we expect from formula (8) that they should have very different consequences on the evolution of the system, in the sense that a positive Coulomb stress perturbation leads to an instantaneous acceleration of sliding on the fault, whereas a negative Coulomb stress perturbation might generate an instantaneous deceleration of the fault. More details about this instantaneous effect are provided by *Linker and Dieterich* [1992] and *Perfettini et al.* [2003].

[19] Motivated by the results of *Dublanchet et al.* [2013], we used in our simulations different antiasperity dimensions

that correspond to different asperity densities according to equation (6). *Dublanchet et al.* [2013] indeed show that if the relative proportion of seismic material within the fault zones (i.e., the density of asperities) exceeds some threshold that depends on the stability of the creeping material, the successive failures of the asperities destabilize the entire fault and result in a major event that ruptures seismically the creeping barriers. Therefore, we test the effect of a stress perturbation on both subcritical systems characterized by a low asperity density, then on supercritical systems characterized by a large asperity density. Following *Dublanchet et al.* [2013], the two different systems analyzed here are characterized by $\rho < \rho_c$ and $\rho > \rho_c$, where ρ_c is the critical density of asperities defined by *Dublanchet et al.* [2013] and given by

$$\rho_c = \left[1 + \frac{\Delta\tau_0}{(a-b)_s \sigma \ln(v_{sis}/v_p)}\right]^{-1}, \quad (9)$$

where $\Delta\tau_0$ is the mean stress drop on the asperity and v_{sis} is the threshold of sliding velocity allowing the dynamic effects to dominate over the direct effect of rate-and-state friction so that radiation of seismic waves might occur. With our choice of parameters, and assuming like *Rubin and Ampuero* [2005] that $v_{sis} = v_{dyn} = a\sigma/\eta$, we end up with $v_{sis} \sim 2$ cm s^{-1}. In order to extend our study to different values of ρ_c, we also tested different values of a_s and b_s parameters.

4. Results

4.1. Subcritical Versus Supercritical Response

[20] The results presented in Figure 2 illustrate the two different regimes of behavior that characterize the asperity surrounded by creep in response to an instantaneous stress perturbation. The main result shown in Figure 2a concerns the cumulative displacement at the center of the asperity showing that in the subcritical density of asperities case, a stress perturbation leads to an instantaneous increase (if $\Delta cff > 0$) or decrease (if $\Delta cff < 0$) in the seismicity rate, followed by a transient return to the background rate. This evolution of seismicity rate is very similar to the change in the rhythm of the repeaters observed by *Lengliné et al.* [2009] at Parkfield in response to the coseismic stress perturbation induced by the 2004 M_w6 earthquake. On the other hand, in the supercritical case, if the stress perturbation induces an advance (if $\Delta cff > 0$) or a delay (if $\Delta cff < 0$) in the first rupture as expected in a Coulomb failure model, the figure suggests that the underlying transient duration is shorter than the recurrence time.

[21] Furthermore, as shown in Figures 2b and 2c, the stress perturbation is relaxed in very different ways for the subcritical and the supercritical systems. In the subcritical configuration, the evolution of the mean cumulative displacement shows that the entire fault plane continuously slips between seismic events on the asperity so that the stress perturbation is continuously released. This behavior arises because of the large proportion of aseismic segments on the fault surface that are never locked. On the other hand, the supercritical systems only releases stress during the seismic events on the asperity that destabilizes the creeping barriers,

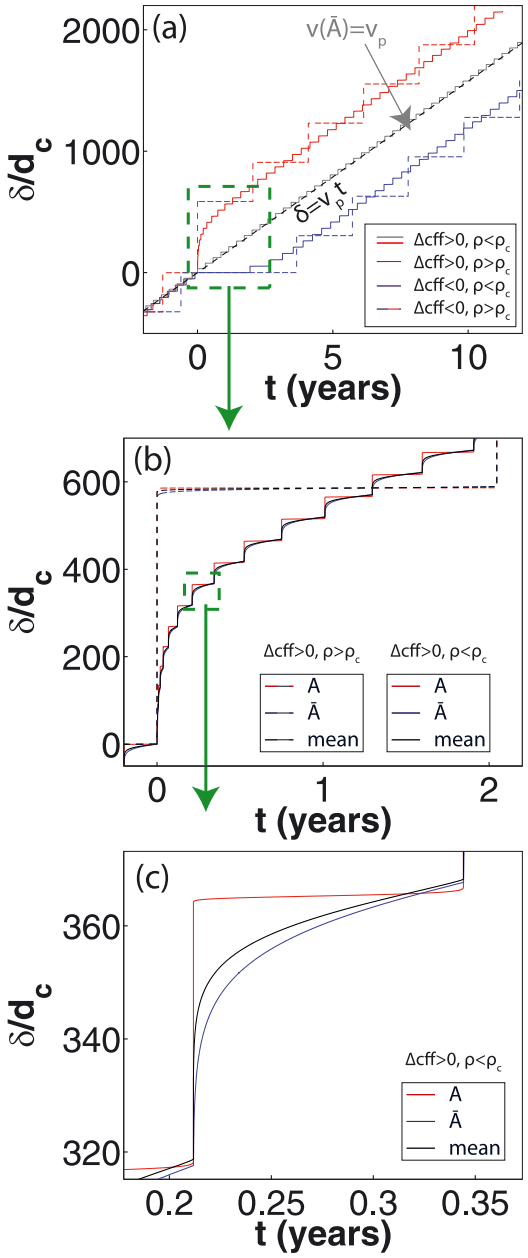

Figure 2. (a) Normalized cumulative displacement δ/d_c of a point at the center of the asperity as a function of time t. The system is instantaneously perturbed at $t = 0$ years. Red curves indicate the results obtained for a positive Coulomb stress perturbation. Blue curves correspond to a negative Coulomb stress step. The solid red curve correspond to simulation 3 of Table 2, the dashed red curve is simulation 16, the solid blue curve is simulation 13, and the dashed blue curve is simulation 17. The solid gray curve indicates the response of the system $\rho/\rho_c = 0.3$ to $\Delta cff = 0.8$ MPa, when the sliding velocity on the antiasperity $\bar{A}$ is maintained at the loading rate v_p (no transient). Black dashed line is the load point displacement at v_p. (b and c) Details of the cumulative displacement shown in Figure 2a, on a point of the asperity A (red curves), on a point of the antiasperity $\bar{A}$ (blue curves), and spatially averaged cumulative displacement (black curves). In all the figures, solid curves indicate $\rho < \rho_c$ and dashed curves correspond to $\rho > \rho_c$.

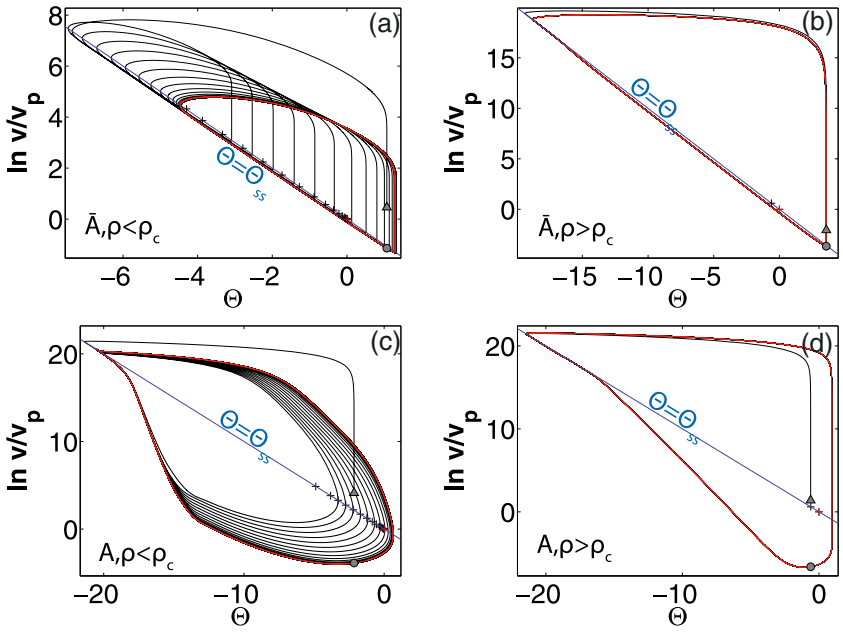

Figure 3. Phase diagrams corresponding to the evolution of a point (a and b) on the antiasperity and (c and d) at the center of the asperity in the $(\ln v/v_p, \Theta)$ space, in response to an instantaneous Coulomb stress step of 0.8 MPa. A and $\bar{A}$ in the bottom left corner indicate, respectively, asperity and antiasperity. Figures 3a and 3c correspond to a subcritical density of asperities $\rho = 0.3 < \rho_c$ (simulation 3 in Table 2), and Figures 3c and 3d represent the response of a system characterized by a supercritical density of asperities $\rho = 0.55 > \rho_c$ (simulation 16 in Table 2). Red curves highlight the limit cycle characterizing the unperturbed system. Gray dots indicate the values of the variables at the instant of perturbation, and gray triangles correspond to the perturbed values of the variables just following the stress step. Subsequent evolution is represented by black solid curves. Blue solid lines indicate the position of steady state points according to the rate-and-state friction law. Steady state variables are labeled with ss subscripts. Black crosses indicate the values of $\ln v/v_p$ and Θ averaged both in time (over one seismic cycle) and in space (over the whole fault area). The red cross is the mean position of the unperturbed cycle.

and the average creep on the entire fault vanishes during interseismic periods.

[22] As another way to represent the effect of the two perturbations, we plotted the evolution of the two kinds of asperities (either with a large or a small antiasperity) in a $(\Theta, \ln v/v_p)$ phase space. The results are shown in Figure 3 for the response to the shear stress step and in Figure 4 for the response to the normal stress step. Since our model couples a velocity weakening asperity with velocity strengthening behavior, we represented the evolution of two representative points of the fault: one at the center of the asperity characterizing the behavior of the velocity weakening asperity and one on the creeping part of the fault that gives some insights into the behavior of the creeping portions of the fault. In both cases of stress perturbations, the subcritical system (characterized by $\rho < \rho_c$) instantaneously moves out from the unperturbed seismic cycle and comes back to this cycle after several oscillations around the steady state line. This evolution characterizes both the creep response and the asperity response. On the contrary, the response of the supercritical system ($\rho > \rho_c$) is slightly different: The first rupture occurs on a path that lies outside the limit cycle, but afterward, the system never deviates from it. This latter characteristic illustrates the same observation as what was outlined by the cumulative displacement evolution in Figure 2. We will later come back to this representation to give more details about the evolution right after the main perturbation.

[23] One of the most important result presented in Figure 2a is that the Omori decay observed in the rupture of the asperity in the subcritical case is no more present when the sliding velocity on the strengthening segments of the fault is imposed at the loading rate v_p (gray curve in Figure 2a). For that reason, we propose that the relaxation of the system observed for subcritical density of asperities is a consequence of a transient accelerated (or decelerated) deformation occurring on the strengthening segments of the system in response to the stress perturbation that in turn amplifies the tectonic stressing on the asperity. This is also suggested by Figures 3a and 4a showing that the mean sliding velocity on the antiasperity region is suddenly increased (or decreased) by the stress perturbation and relaxes back to its unperturbed level. These simulations thus support the model proposed by *Schaff et al.* [1998] and *Bourouis and Bernard* [2007] in which the Omori decay on the asperity is forced by the transient acceleration and deceleration of the creep. However, as this is pointed out by the results of Figures 2, 3, and 4, this creep control of the slip relaxation is only possible in subcritical systems, that is, in the case of a large enough creeping antiasperity. Otherwise, the stress perturbation only induces an alteration of the time to failure. In this latter situation, the asperity entirely controls the evo-

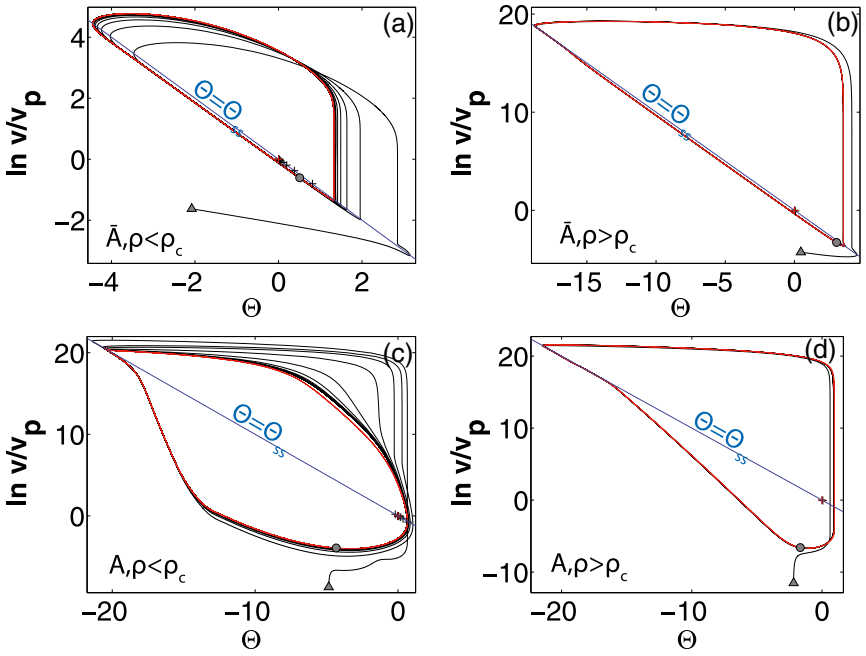

Figure 4. Same diagrams as in Figure 3 but for an instantaneous negative Coulomb stress perturbation of –0.8 MPa. The results correspond to simulations 13 and 17 in Table 2. (a and b) Characteristic evolution of the antiasperity after the stress step in the case $\rho < \rho_c$ and $\rho > \rho_c$. (c and d) Characteristic response of the asperity in the case $\rho < \rho_c$ and $\rho > \rho_c$.

lution of the system. Moreover, once a source fails, the fault loses the memory of the stress perturbation, and the next rupture on this source occurs after the unperturbed recurrence time, preventing the occurrence of an Omori decay at the scale of a single fault, or a single asperity.

[24] In the following section, we will focus on subcritical faults characterized by $\rho < \rho_c$, and we will investigate how ρ influences the relaxation process of the asperity surrounded by aseismic creep in response to a Coulomb stress perturbation.

4.2. Omori Law for $\rho < \rho_c$

[25] In the previous section, we have identified the antiasperity creep transient excited by the stress step as the main mechanism forcing the asperity to rupture in an Omori process. According to *Ziv* [2007] and *Perfettini and Ampuero* [2008], the acceleration of slip associated with a positive stress perturbation on a velocity strengthening fault segment is initially localized over a patch which dimension is on the order of $L_{bs} = Gd_c/b_s\sigma$ and then expands as a quasi-static crack. Consequently, such transient might occur in our model only if the velocity strengthening segments have a characteristic dimension larger than L_{bs}, which is equivalent to a small enough effective stiffness. This latter condition is similar to what is inferred by *Helmstetter and Shaw* [2009] for the velocity strengthening spring and slider system that could experience creep transients only if its stiffness k is smaller than $k_b = b\sigma/d_c$. In our simulations, L_{bs} is always smaller than 60 m which is less than the minimum fault dimension used (see Table 1), and the condition highlighted by *Ziv* [2007] and *Perfettini and Ampuero* [2008] never prevents the occurrence of a creep transient, even for subcritical density of asperities. Furthermore, we expect from elasticity that the larger the creeping antiasperity is, the stronger the amplification of stress perturbation on the asperity is.

[26] In order to quantify this effect, we reported in Figure 5 the evolution of the cumulative displacement averaged over the entire fault and the corresponding seismicity rate generated by the successive ruptures on the asperity, for the simulations 1 to 6 and 11 to 15 of Table 2. In Figure 5, the timescale is normalized using the characteristic time t_{r0} of the relaxation of a velocity strengthening spring and slider system at steady state [*Marone et al.*, 1991; *Perfettini and Ampuero*, 2008; *Helmstetter and Shaw*, 2009]. t_{r0} is given by

$$t_{r0} = \frac{(a-b)_s \sigma w}{G v_p}, \tag{10}$$

where $(a - b)_s$ is the steady state friction parameter characterizing the strengthening parts of the fault. Our choice of t_{r0} is motivated by the results of Figures 3a and 4a where the relaxation of the creep driving the Omori decay on the asperity occurs along the steady state line. Therefore, we expect that the characteristic duration of the Omori decay is on the order of t_{r0}. Furthermore, we normalized the seismicity rate by its background value $r_0 = 1/T$, T being the unperturbed seismic cycle duration under loading at constant rate.

[27] For all the values of ρ used in these simulations, the spatially averaged cumulative displacement δ reaches a steady state regime defined by

$$\delta(t) = v_p t + \frac{\Delta cff}{k}, \tag{11}$$

with k being the stiffness of the elastic medium of thickness w, that is, $k = G/w$. This regime corresponds to an average cumulative displacement that balances the loading displacement at v_p with a delay introduced by the stress perturbation.

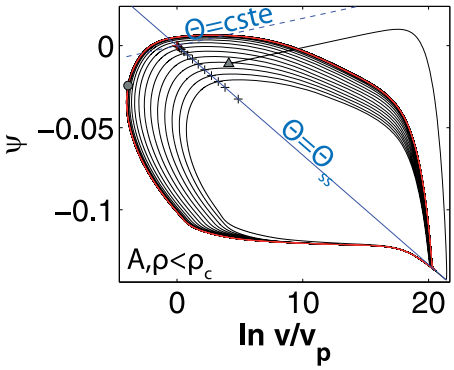

Figure 5. Characteristic phase diagram of the asperity in the $(\ln v/v_p, \psi)$ space, where $\psi = (\tau - \mu_0\sigma)/\mu_0\sigma$ is the normalized shear stress, for the simulation presented in Figures 3a and 3c. The different symbols and colors have the same meaning as in Figures 3 and 4. Dashed blue line indicates a constant state variable trajectory.

The differences between the simulations arise in the short time seismicity rate, and in the timescale of the relaxation toward the steady state regime. In particular, for small values of ρ, the asperity is weakly activated but the Omori law takes more time to attenuate. On the other hand, for large values of ρ, the short time response is stronger but the Omori decay is shorter, so that the total number of earthquakes occurring in the Omori law until the global steady state is approximately constant and independent of ρ. The resulting step in cumulative slip reaches $\Delta cff/k$ in each case.

[28] In order to understand the frictional evolution of the system after the perturbation, for both the asperity and the antiasperity, we will focus again on Figures 3a, 3c, 4a, and 4c. The typical response of the antiasperity shown in Figures 3a and 4a could be described as follows: After an early evolution leading to the first seismic rupture of the asperity, the creeping parts of the fault evolve along the steady state line back to the initial velocity level. This long-term evolution at steady state is expected for a perturbed single degree of freedom elastic system obeying velocity strengthening friction [*Perfettini and Ampuero*, 2008; *Helmstetter and Shaw*, 2009]. The major difference with the single degree of freedom system is that during this relaxation, the creep forces the asperity and is in turn periodically excited by the failure of the asperity. This latter rupture is apparent in the phase diagrams since it generates an instantaneous positive shear stress perturbation that induces an acceleration at almost constant state, as mentioned in the previous sections. Therefore, the relaxation of the creep transient on the surroundings of the asperity has two components: The first one is a steady state relaxation and the second one is a periodic oscillation around this steady state line. The periodic oscillation has a shape similar to the unperturbed limit cycle but its size evolves as it is shifted along the steady state line. In other words, in response to a stress perturbation and after an early evolution, the sliding velocity of the creeping parts of the fault oscillates around a mean level that is either larger than the mean level of the unperturbed cycle or lower than this. This mean level determines if the asperity is forced at a higher or lower rate than in the unperturbed cycle. The asperity also reacts in a similar way, as presented in Figures 3 and 4: The perturbation moves the system away from the unperturbed cycle, and the system evolves afterward on trajectories that correspond to scaled versions of the unperturbed cycle shifted along the steady state line. In addition to the trajectories computed for an asperity and an antiasperity point, we also computed the evolution of the mean levels of v and Θ characterizing the shift of the cycle in the phase diagrams and averaged over the fault plane. The results are represented by the black crosses in Figures 3 and 4: In each case of perturbation, the mean variables describing the fault evolve along the steady state line toward their unperturbed values.

[29] Based on this analysis of the phase diagrams and assuming that relaxation of the system occurs through trajectories that are scaled versions of the unperturbed seismic cycle of the asperity, we derive in Appendix B a theoretical model that leads to the following expression of the mean cumulative displacement $\bar{\delta}(t)$ on the asperity (that also corresponds to the mean displacement of the entire fault plane) as a function of time t following the stress perturbation:

$$\bar{\delta}(t) = v_p t_r \ln\left[1 + e^{\Delta cff/A\sigma_1}(e^{t/t_r} - 1)\right], \tag{12}$$

where A is the average value of the friction parameter $a - b$ over the fault plane, σ_1 is the normal stress right after the stress perturbation, and t_r is a characteristic time corresponding to the duration of the transient experienced by the fault that in turn depends on A in the following way:

$$t_r = \frac{A\sigma_1}{k v_p}. \tag{13}$$

The relaxation process is therefore analog to the relaxation of a fault characterized by an effective steady state friction parameter A. The derivation presented in Appendix B is valid as long as $\rho < \rho_c$. Furthermore, from the phase diagram presented in Figure 6, the stress drop $\Delta\tau_0$ on the asperity (i.e., the vertical extent of the seismic cycle) is approximately given by $(b-a)_w\sigma \ln v_{sis}/v_p$, since the extreme points of the trajectories lie in the vicinity of the steady state line. Such a scaling of the stress drop is similar to what was inferred by *Tse and Rice* [1986] in the case of a spring and slider system. Making use of this scaling in the expression of the critical density of asperities (9) leads to

$$\rho_c = \left[1 - \frac{(a-b)_w}{(a-b)_s}\right]^{-1}. \tag{14}$$

Thus, for the fault considered here, $\rho < \rho_c$ reduces to $A > 0$, from the definition (B7) of A.

[30] From the expression (12) of the cumulative mean displacement on the fault, it is possible to derive an expression of the normalized seismicity rate r/r_0. For that, we will first neglect the small variation of the stress drop that occurs for the first aftershocks (corresponding to the reduction of the vertical extent of the seismic cycle in Figure 6). We will further discuss this latter effect in the discussion section. Then, we will assume that the seismicity rate varies slowly, that is, on a timescale much larger than $t_a = a_w\sigma/\dot{\tau}$, the characteristic relaxation time of the asperity defined by *Dieterich* [1994]. *Helmstetter and Shaw* [2009] indeed shows that under these latter assumptions, the model of

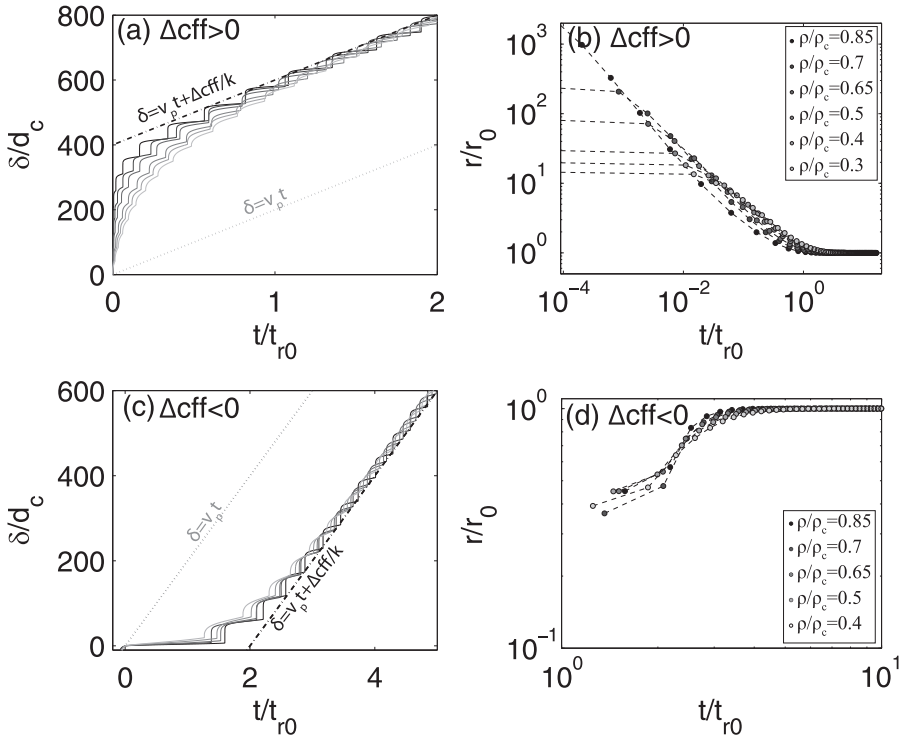

Figure 6. (a and b) Normalized cumulative displacement δ/d_c averaged over the fault plane with an asperity embedded in a creeping fault segment and normalized seismicity rate r/r_0 recorded on the asperity in response to a positive Coulomb stress perturbation Δcff = 0.8 MPa versus normalized time t/t_{r0} from the onset of the stress step. t_{r0} is the characteristic timescale for the relaxation of creeping segments defined by equation (10), and r_0 is the background seismicity rate produced by the asperity under loading at constant rate v_p. The different curves correspond to different values of subcritical asperity density ρ reported in Figure 6b. These results correspond to the simulations 1 to 6 in Table 2. Gray dotted line and black dashed line in Figure 6a indicate loading at v_p before and after the stress step, respectively. $k = G/w$ is the stiffness of the medium in the fault normal direction. (c and d) Same diagrams as in Figures 6a and 6b obtained in the case of a negative Coulomb stress perturbation Δcff = –0.8 MPa (simulations 11 to 15 in Table 2). The different values of asperity density used in Figures 6c and 6d are labeled in Figure 6d.

Dieterich [1994] reduces to a seismicity rate proportional to the stressing rate acting on the asperity. In our model, the characteristic time for seismicity rate variations is approximately t_r, and the seismicity rate is proportional to the stressing rate as long as $t_r/t_a \gg 1$. Such a condition might be violated for density of asperities close to critical, that is, when A and thus t_r nearly vanish. However, we will assume in the following that this is not the case, and we will derive the seismicity rate from the expression of the stressing rate on the asperity. Following *Lengliné et al.* [2009], this latter forcing term is made of two contributions: the loading at v_p imposed at $w/2$ in the fault normal direction and the stressing associated with slip on the antiasperity, so that

$$\dot{\tau} = kv_p + k_a v_a, \tag{15}$$

where $k = G/w$ is the stiffness of the elastic medium defined earlier, v_a is the mean sliding velocity on the antiasperity, and k_a is the stiffness that relates slip on the antiasperity to stress on the asperity. This latter term strongly depends on the geometry of the system. It turns out that when averaged over one seismic cycle, the stressing rate could be rewritten in the following form:

$$\dot{\bar{\tau}} = kv_p + k_a \dot{\bar{\delta}}(t), \tag{16}$$

where $\bar{\delta}(t)$ is given by equation (12). In the absence of any stress perturbation, the stressing rate $\dot{\bar{\tau}}$ becomes

$$\dot{\bar{\tau}} = \dot{\bar{\tau}}_0 = (k + k_a)v_p, \tag{17}$$

and assuming proportionality between seismicity rate r and stressing rate $\dot{\bar{\tau}}$ (for a constant stress drop), we end up with the following expression:

$$\frac{r}{r_0} = \frac{\dot{\bar{\tau}}}{\dot{\bar{\tau}}_0} = \frac{k/k_a}{1 + k/k_a} + \frac{1}{1 + k/k_a}\frac{\dot{\bar{\delta}}(t)}{v_p}, \tag{18}$$

where r_0 is the background seismicity rate in the absence of perturbation. In order to simplify equation (18), we show in Appendix C that for a small density of asperities, $k/k_a \ll 1$, so that we end up with

$$\frac{r}{r_0} = \frac{\dot{\bar{\delta}}(t)}{v_p} = \left[\left(e^{-\Delta cff/A\sigma_1} - 1\right)e^{-t/t_r} + 1\right]^{-1}. \tag{19}$$

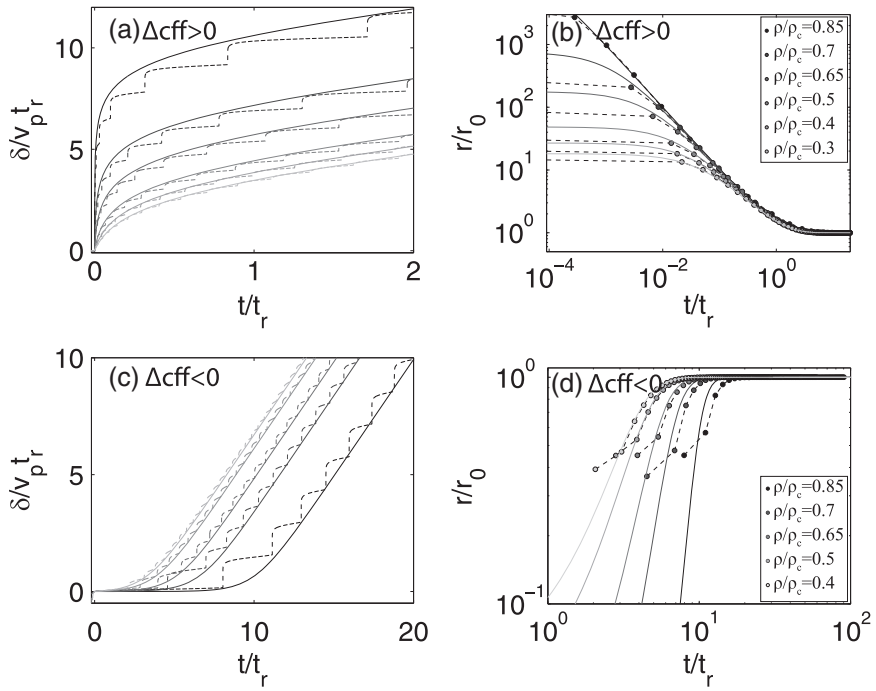

Figure 7. Same diagrams as in Figure 6 but with a different normalization of the mean cumulative displacement δ and time t following the onset of the stress perturbation. In this figure, v_p is the background constant loading rate, and t_r is the characteristic timescale given by equation (13). Dashed curves plotted in Figures 7a and 7c correspond to the numerical results, as well as dashed lines and circles in Figures 7b and 7d. Solid lines in Figures 7a and 7c are the analytical approximation (12) for the mean cumulative displacement of the system. Solid lines in Figures 7b and 7d correspond to the analytical expression (19) derived from (12) for the seismicity rate decay after a Coulomb stress perturbation.

Note that equation (19) is similar to the expression derived by *Dieterich* [1994] in the case of a population of self-accelerating spring and sliders, provided that the a parameter of the asperity is replaced by the effective $a - b$ parameter.

[31] The numerical results and the theory developed in this section are in rather good agreement as shown in Figures 7: equations (12) and (19) correctly predict the mean evolution of the asperity surrounded by a region of aseismic creep after a Coulomb stress perturbation, at least after the first seismic event on the asperity. Moreover, the asymptotic regime is in agreement with equation (B13). This agreement between the numerical results and the theoretical expressions (12) and (19) is further supported by the collapse of all the numerical solutions from simulations 1 to 8 and 11 to 15 shown in Figure 8. In this latter figure, the normalized averaged cumulative displacement $\bar{\delta}/v_p t_r$ is represented as a function of ξ and the normalized seismicity rate r/r_0 as a function of ζ, with ξ and ζ being given by

$$\xi = e^{\Delta cff/A\sigma_1}\left(e^{t/t_r} - 1\right), \tag{20}$$

$$\zeta = \left(e^{-\Delta cff/A\sigma_1} - 1\right) e^{-t/t_r}, \tag{21}$$

so that expressions (12) and (19) become

$$\frac{\bar{\delta}}{v_p t_r} = \ln(1 + \xi), \tag{22}$$

$$\frac{r}{r_0} = \frac{1}{1 + \zeta}. \tag{23}$$

5. Discussion

5.1. Frictional Condition Allowing Creep Control of Omori Decay

[32] In the previous sections, we presented numerical results and an analytical approach that provide some understanding about how an asperity surrounded by a creeping region responds to an instantaneous stress perturbation. In particular, the model derived in this study implies that a creeping fault hosting one seismic asperity releases a stress perturbation by slipping with a mean frictional resistance that only depends on the mean sliding velocity v on the fault, through an effective friction parameter A, defined as the mean value of rate-and-state $a - b$ parameter over the fault area. This concept of an effective friction parameter controlling the relaxation of an asperity surrounded by creep has already been proposed by *Bourouis and Bernard* [2007]. Our study therefore provides the theoretical basis of their conceptual model.

[33] As another implication of our model is that when the effective friction coefficient A is positive (or equivalently the density of asperities is subcritical $\rho < \rho_c$), the fault zone is velocity strengthening on average, and the seismicity rate recorded on the asperity follows the mean decay of the slip velocity on the fault that is apparently similar to the relaxation process of a velocity strengthening spring and slider system, leading to a strong correlation between postseismic afterslip and seismicity rate decay. However, this decay is not directly controlled by the friction param-

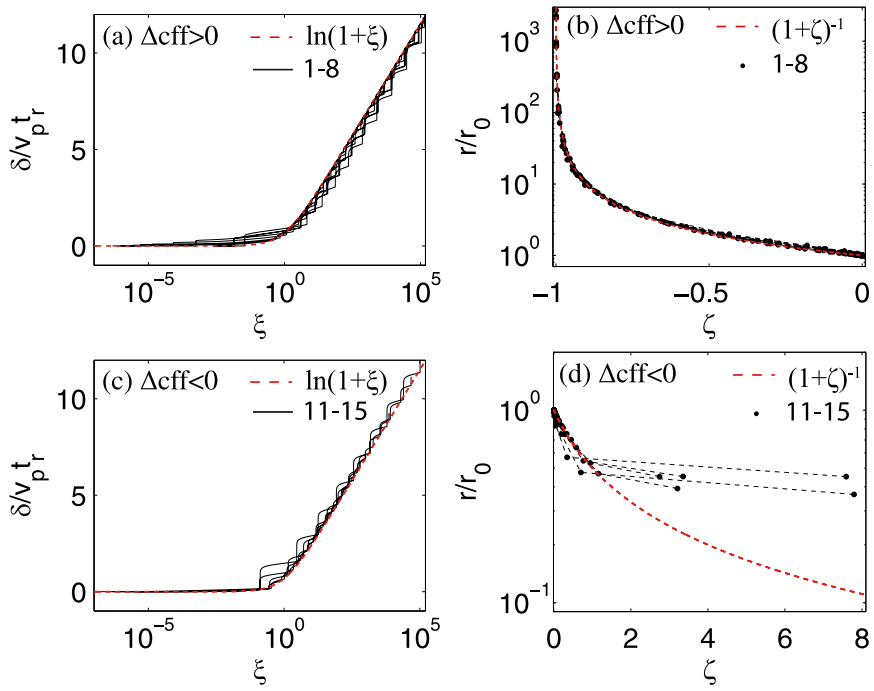

Figure 8. Same diagrams as in Figure 7, where the mean cumulative displacement is plotted as a function of ξ defined by equation (20), and the seismicity rate represented as a function of ζ defined by equation (21). The black curves represented in Figures 8a and 8b correspond to the numerical results of simulations 1 to 8 in Table 2. The black curves in Figures 8c and 8d correspond to the results of simulations 11 to 15 in Table 2. The heavy red dashed lines correspond to the analytical expressions (22) and (23).

eters of the creeping areas of the fault, but rather by the mean steady state friction parameter $a - b$ on the fault. This should be kept in mind for estimates of the friction parameter $(a - b)$ from geodetic and seismicity analysis of postseismic deformation.

[34] On the other hand, if the effective friction parameter A is negative (corresponding to $\rho > \rho_c$), the asperity surrounded by creep is on average velocity weakening, and there is no correlation between the relaxation of the creeping segment and the seismicity rate produced by the asperity. In this frictional regime, the occurrence of an Omori law is better explained by the model of *Dieterich* [1994] that involves a population of such velocity weakening asperities.

[35] The present study formalizes the creep controlled seismicity model proposed by *Schaff et al.* [1998], *Perfettini and Avouac* [2004], and *Bourouis and Bernard* [2007], since it provides a theoretical and a numerical basis for this concept, as well as the frictional conditions allowing this mechanism. Furthermore, our model extends the work of *Dublanchet et al.* [2013], in the sense that the critical density of asperities defined by these authors in the case of faults with multiple asperities is equivalent to the transition between effective velocity weakening behavior $A < 0$ and effective velocity strengthening $A > 0$ behavior. In other words, the creep control of both background seismicity and aftershock sequences occurs only for subcritical density of asperities, or equivalently for effective velocity strengthening frictional properties.

5.2. How to Interpret Aftershock Sequences: The Example of Parkfield Repeaters After the 2004 M_w6 Event

[36] In the framework developed here, it is possible to extend the interpretation of the sequence of the Parkfield repeaters after the September 2004 M_w6 event already analyzed by *Lengliné et al.* [2009], since it provides a way to interpret the parameters of the postseismic transient forcing the asperities in terms of average local frictional strength. In their modeling approach, *Lengliné et al.* [2009] assume, in addition to the tectonic loading, a postseismic transient associated with the M_w6 event, generating on each repeating asperity an additional stress of the form $\sigma_{post}(t) = A_0 \ln(1 + t/t_0)$, t being the time since the main shock, and t_0 the characteristic duration of the postseismic deformation. In our model, this latter term corresponds to $k_a\bar{\delta}(t)$ where k_a is the equivalent stiffness corresponding to the mean elastic interaction between asperity and antiasperity. Using equation (12) along with the condition $t \ll t_r$, $k_a\bar{\delta}(t)$ reduces to

$$k_a\bar{\delta}(t) \sim k_a v_p t_r \ln\left[1 + e^{\Delta cff/A\sigma_1}\frac{t}{t_r}\right], \tag{24}$$

which is of the same form as the $\sigma_{post}(t)$ term of [*Lengliné et al.*, 2009], provided that

$$t_0 = t_r e^{-\Delta cff/A\sigma_1}, \tag{25}$$

$$A_0 = k_a v_p t_r. \tag{26}$$

The new timescale t_0 emerging here is slightly different from t_r: t_0 controls the shape of the Omori decay (or the instantaneous stressing rate) right after the perturbation, whereas t_r indicates the duration of the relaxation process. Furthermore, using the scaling provided in Appendix C for k_a, the expression of A_0 becomes approximately

$$A_0 = \frac{w}{4R}(1 + 2\alpha_0)A\sigma_1, \tag{27}$$

where α_0 is the nondimensional function of Lame parameters defined in Appendix C.

[37] *Lengliné et al.* [2009] estimate the mean value of A_0 to be around $(1.4 \pm 0.9)\Delta\tau_0$, $\Delta\tau_0$ being the mean stress drop on Parkfield asperities. Assuming $\Delta\tau_0 \sim 3$ MPa, $R \sim 30$ m, $w \sim 3$ km and $\sigma_1 \sim 100$ MPa as relevant orders of magnitudes for these quantities in Parkfield, as shown in the model description section, we end up with a mean value for the local friction parameter of $A = 7 \pm 4.10^{-4}$. Furthermore, in the estimation of *Lengliné et al.* [2009], the values of t_0 span almost 5 orders of magnitudes depending on the repeater analyzed, and they attribute this scattering to a heterogeneous postseismic deformation along San Andreas fault. However, according to the scaling given by equation (25), an alternative interpretation would be to consider the heterogeneous cosesimic stress perturbation along the fault. Making use of the same orders of magnitude than previously, and using $A = 0.0007$ as a rough estimate of the friction parameter A, equation (25) leads to t_0 spanning almost 60 orders of magnitudes as Δcff varies between $-2\Delta\tau_0$ and $0.8\Delta\tau_0$ as assumed by *Lengliné et al.* [2009]. This is slightly larger than what is inferred by *Lengliné et al.* [2009] (t_0 varying approximately from 0.16 to 23 days).

[38] Another explanation of this scattering in the values of t_0 would be a heterogeneity in the average friction parameter A. This latter explanation would imply according to the definition of A either a heterogeneity in the friction parameters a and b along the fault or a heterogeneous local density of asperities ρ. If we consider a much smaller range in the values of the coseismic stress perturbations Δcff than what is inferred by *Lengliné et al.* [2009], varying for instance from $-0.05\Delta\tau_0$ to $0.05\Delta\tau_0$, and a friction parameter ranging between 0.0003 and 0.0011 as estimated previously, we end up with t_0 between 0.2 days and 13 years that is still in agreement with the estimation of *Lengliné et al.* [2009]. Thus, even with an underestimation of the coseismic perturbation spatial heterogeneity in Parkfield, the scattering in the values of t_0 could be explained by a distribution of the effective friction parameter A that deviates less than 60% from the mean value. This scattering in A could reflect different local density of asperities, that is, different dimensions of the velocity strengthening environments of the asperities along the San Andreas Fault.

[39] In any case, the model presented in this study does not allow to model real repeater sequences because of the unrealistic periodic boundary conditions used. This issue requires to develop further the numerical model in a way that is suggested in the generalization section of the discussion. Nevertheless, as mentioned in the second section, the periodic case could approximate constantly sliding boundaries if the asperity is weakly sensitive to the ruptures of its replicas, which is achieved for a very sparse distribution of asperities. In order to estimate the maximum spacing of asperities allowing to neglect the effect of the replicas, we consider a set of circular asperities of radius R distributed on a cartesian grid of unit spacing L, experiencing a simultaneous sliding Δu. Each asperity could be considered isolated as long as the rupture of the first neighboring asperity generates a stress perturbation of much smaller amplitude than the stress drop of each asperity. According to *Maruyama* [1964], two neighboring asperities separated by L generate on each other a stress perturbation τ_n of the order of $\tau_n \sim G\Delta u\pi R^2/L^3$. Similarly, the stress drop $\Delta\tau_0$ on the asperity associated with the slip Δu is of the order of $\Delta\tau_0 \sim G\Delta u/R$. From these orders of magnitude, τ_n is a small fraction of $\Delta\tau_0$, and the effect of the replicas is negligible as long as $(R/L)^3 \ll 1$.

5.3. Timing of the First Rupture and Long-Term Relaxation

[40] In this study, we were only interested in the long-term behavior of the asperity, that is, at a timescale longer than the interevent delay, and therefore, our theory does not explain how a stress perturbation delays or advances the first rupture of an asperity surrounded by creep. As mentioned in the introduction, this problem has been partly addressed by *Perfettini et al.* [2003] and more recently by *Kaneko and Lapusta* [2008] who studied the effect of a Coulomb stress perturbation on the time to failure in two dimensional models of faults that include depth variable friction properties with a transition between velocity weakening and velocity strengthening behavior. The conclusion of *Kaneko and Lapusta* [2008] that creeping segments of the fault might affect the timing of the first rupture on the fault is similar to our model where the extent of creeping surroundings of the asperity influences the long term relaxation of the fault. For that reason, we expect that for $\rho < \rho_c$, the timing of the first rupture in our model might also be controlled by ρ, or more precisely by the average friction coefficient A.

5.4. Stress Step Amplitude

[41] One of the main results highlighted by our simulations is the existence of two distinct regimes of activity in response to a stress perturbation on an asperity surrounded by creep, depending on the ratio between the area occupied by the asperity and the total area of the fault (i.e., the density of asperities). These distinct regimes consist in either an Omori decay for subcritical density of asperities or a change in a single rupture time for supercritical density of asperities. In this framework, the critical parameter that seems to separate the two possible responses is the ability of the creeping sections of the fault to be destabilized by the rupture of the asperity. However, even if the ruptures of the asperity do not generate destabilizing transients, the onset of an external stress perturbation could temporarily provide the complement of acceleration necessary to reach seismic sliding on the creeping barriers. Two examples of such an intermediate behavior are detailed in Figure 9 and correspond to simulations 9 and 10 conducted on systems characterized by a ratio ρ/ρ_c near 1. The effect of a positive stress perturbation in these conditions results in a transient logarithmic evolution of the mean cumulative displacement that is well captured by equation (12) as shown in Figure 9a. However, the relaxation of the seismicity rate detailed in Figure 9b does not follow equation (19). The misfit arises because as

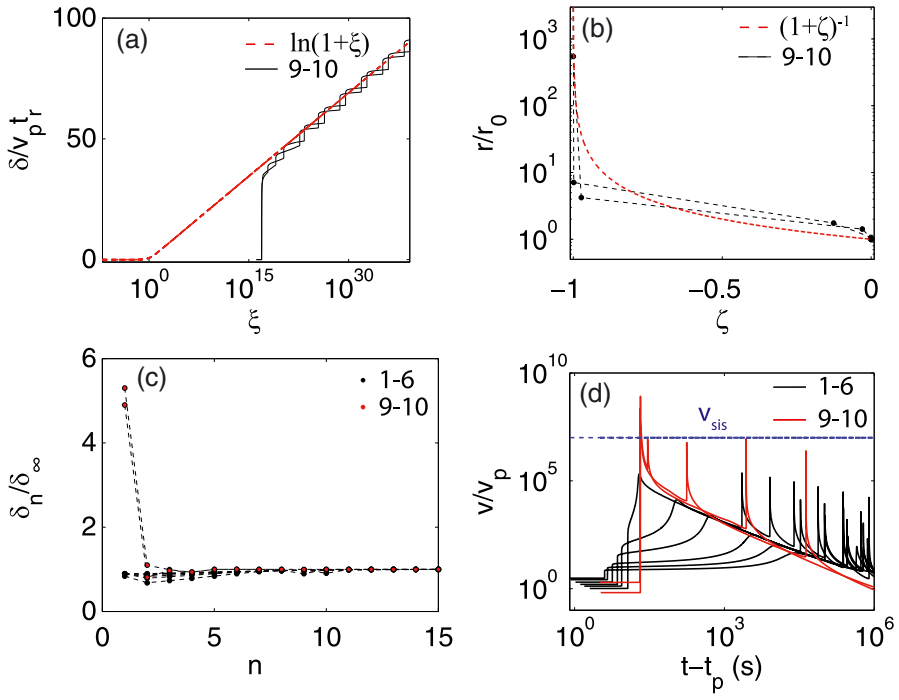

Figure 9. (a and b) Same diagrams as in Figures 8a and 8b for simulations 9 and 10 of Table 2. (c) Spatially averaged cumulative displacement δ_n accumulated on the fault during the seismic cycle n following the onset of the stress perturbation, for simulations 1 to 6 (black dots) and 9 to 10 (red dots) of Table 2. δ_∞ is the value of δ_n in the absence of stress perturbation. (d) Sliding velocity on a point of the antiasperity after the stress perturbation, for simulations 1 to 6 (black curves) and 9 to 10 (red curves) of Table 2. The point considered here is the most distant point from the asperity. t_p indicates the instant of the stress perturbation onset. The blue dashed line indicates the radiative sliding velocity v_{sis} = 1 cm s^{-1}.

shown in Figures 9c and 9d, the first aftershock occurring in the system involves the entire fault plane by destabilizing the creeping barriers and the mean displacement accumulated during this event is at least 5 times larger than the usual slip accumulated during the following events. In these conditions, the proportionality between stressing rate and seismicity rate is no more valid and it is more difficult to derive the seismicity rate from the cumulative displacement on the asperity.

[42] One way to understand such an intermediate behavior is to consider how the critical density of asperities defined in equation (9) could be modified by the occurrence of an external stress perturbation. For a matter of simplicity, we consider a shear stress perturbation of amplitude $\Delta\tau > 0$. This stress increase generates an acceleration of the creep so that the sliding velocity instantaneously moves from v_0 to v_1, where $\ln v_1/v_0 = \Delta\tau/a_s\sigma$. This latter term could be used as a small modification of the $\ln v_{sis}/v_p$ term in the expression of the critical density of asperities (9) that quantifies the amount of acceleration necessary to destabilize the system. We end up with the following expression of the modified critical density of asperities ρ_c^* that account for the external stress perturbation:

$$\rho_c^* = \left[1 + \frac{\Delta\tau_0}{(a-b)_s\sigma\left(\ln\left(v_{sis}/v_p\right) - \Delta\tau/a_s\sigma\right)}\right]^{-1}. \qquad (28)$$

[43] From Table 2, simulations 9 and 10 are conducted on systems characterized by $\rho/\rho_c < 1$ and $\rho/\rho_c^* > 1$ and therefore situated in an intermediate range of asperity density allowing major destabilization with the help of an external stress perturbation. As shown in Figure 9, our theory fails to explain the seismicity generated by such systems.

[44] More generally, we expect that each subcritical system could be destabilized by the onset of a large enough external stress perturbation, which shows that the framework developed in the previous sections is only valid for a limited range of external stress perturbation amplitudes.

5.5. Generalization of the Model

[45] Our model could be generalized to the computation of seismicity in response to any kind of Coulomb stress perturbation, using the framework developed by *Perfettini and Avouac* [2004]. To compute the seismicity rate associated with such perturbations, *Perfettini and Avouac* [2004] indeed use a spring block model at steady state that as we showed above, is perfectly equivalent to what occurs on average for an asperity surrounded by creep, and all the results derived for a spring block model should also apply for the asperity case. Nevertheless, the asperity surrounded by creep could be considered equivalent to a spring and slider system with an effective friction parameter A only at a timescale larger than its own seismic cycle duration. This means that the results developed by *Perfettini and*

Avouac [2004] are only applicable for stress perturbations that evolve with time over a much larger timescale than the period of rupture on the asperity.

[46] One of the assumptions of our study is that the system consisting of an asperity and its creeping surroundings is equivalent to a spring and slider system with an effective friction parameter, and therefore, the length scale characterizing the extent of the creep and asperity system is not present any more in the formulation. Such a length scale is indeed not necessary to explain the numerical results obtained here, since the simulations were conducted with a periodic geometry that is similar to an infinite fault plane, if the truncation is neglected. However, it could be possible to consider that w is an order of magnitude of this length scale, since it controls the average stiffness of the fault considered.

[47] An alternative model would be to consider locked boundary conditions, where the creep and asperity system would be confined in a finite region of characteristic size L, with vanishing slip at a distance larger than $L/2$ from the center of the asperity. From Appendix B, such boundary conditions would introduce an additional term in the expression of the mean elastic stress on the fault (B16) that would prevent the fault to follow the imposed motion at $w/2$ when the global steady state is reached. However, the response of the fault to a stress perturbation (B17) would present the same shape as in the infinite periodic fault (12), with a characteristic duration of Omori law controlled by the effective friction parameter A (or equivalently by the density of asperities). The characterization of this latter behavior requires more numerical investigations, and for the moment, locked boundary conditions cannot be implemented in our numerical model because of periodicity. Nevertheless, it is possible to use approximate locked conditions, by preventing slip on large enough areas between the different images of the fault in the periodic geometry, so that the stressing effect of the multiples on the asperity of interest could be neglected.

[48] Finally, it should be pointed out that the theoretical framework developed in this study relies on the constant seismic cycle shape in the phase diagram during the response to stress perturbations. In a more complex situation involving multiple asperities, the seismic cycle of each source is continuously perturbed by the rupture of the neighboring asperities. Therefore, if the ruptures do not occur in the same order at each seismic cycle, the evolution in the phase diagram is different from what is presented in Figures 3 and 4. This constitutes one of the main limitations of our theoretical approach. However, our model could provide useful insights in the understanding of fault effective friction around isolated and non interacting asperities.

5.6. Nonconstant Stress Drop

[49] The phase diagram of Figure 5 showing the evolution of a characteristic point on the asperity after a positive Coulomb stress step indicates that the stress drop on the asperity is not constant during the postseismic relaxation process. Similarly, in Figure 3, the range of variation of $\ln v/v_p$ and Θ during one seismic cycle right after the stress increase is smaller than in the unperturbed case. This modification evolves to a transient increase of the stress drop back to its background value as the system relaxes to its unperturbed trajectory. This behavior arises from the $\ln v_{\max}/v_{\min}$ dependence of stress drop proposed by *Tse and Rice* [1986] in a spring and slider model. As shown by the results in Figure 3, the maximum velocity $v_{\max}$ reached during each cycle remains constant, but the minimum velocity $v_{\min}$ diminishes. Since the mean velocity during one seismic cycle decays like the seismicity rate, it indicates that the minimum velocity also decays toward its unperturbed value, leading to the observed tendency of the stress drop.

[50] Thus, the stress perturbation promotes a transient modification of the stress drop that relaxes as the mean value of the slip velocity decreases over the timescale t_r. Such a transient modification of the stress drop that correlates with the increase of recurrence time of earthquakes has already been inferred for repeaters located on the Calaveras fault by *Vidale et al.* [1994] and in the laboratory by *Marone* [1998]. In all these studies, the physical reason invoked is the time dependence of healing process on the asperities at low sliding velocity. Since rate-and-state friction accounts for healing through stationary contact, it is not surprising to observe this effect in our numerical simulations.

6. Conclusion

[51] By using numerical simulations with a 3-D rate-and-state asperity model and theoretical considerations on average frictional resistance, we showed in this study that creep control of aftershock sequences at the scale of a single asperity surrounded by aseismic creep in response to a coseismic stress increase is only possible if the effective mean friction coefficient A is positive, or, equivalently, when the asperity density is lower than a critical value. In this frictional regime, the fault segment embedding the asperity is velocity strengthening on average, and its response to a stress perturbation depends on the relative proportion between seismic and aseismic areas, that is on the local density of asperities. These latter results have major implications concerning the understanding of frictional behavior of faults since they allow to infer local effective friction coefficient from the analysis of seismic sequences on isolated repeaters, like in the case of the Parkfield region, but more generally in all multiplet prone areas.

Appendix A: Determination of the Grid Size h

[52] One of the requirements of our modeling approach is to allow for a correct description of the process zone. Following *Ampuero and Rubin* [2008b], for the slip version of the state evolution law and for the friction parameters a and b assumed in this study (characterized by $a/b = 0.2$), the grid cell size has to be much smaller than L_b' given by equation (4), as mentioned in the main text. In this section we conducted some numerical resolution tests with varying grid size h in order to determine the largest value of h allowed to obtain the most accurate description of a seismic cycle on the asperity. For that we used the asperity defined in the main text surrounded by a creeping region so that the density of asperities is $\rho = 0.3$, and we computed the sliding velocity, stress, and state evolution at the center of the asperity and on a point of the antiasperity under tectonic loading at constant rate. We then compared the resulting phase diagrams in Figure A1, because the main developments of this study rely on the analysis of this kind of representation.

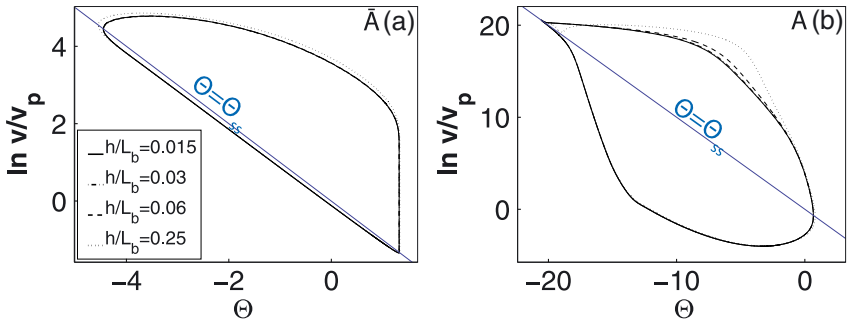

Figure A1. Phase diagrams showing in black the (a) trajectory of an antiasperity typical point and the (b) trajectory of the center of the asperity in the $(\Theta, \ln v/v_p)$ space when the fault is loaded at constant rate v_p. A and $\bar{A}$ refer to asperity and antiasperity, respectively. The different symbols indicate different spatial resolutions h/L_b, h being the computational grid cell size. Blue solid line indicates steady state friction.

The seismic cycle computed appears to remain stable in the phase space when changing h/L_b from 0.03 to 0.015. Therefore, we assumed in the following $h/L_b = 0.03$ provides a correct resolution for our application.

Appendix B: Post Seismic Sliding of an Asperity Surrounded by Creep

[53] In this section, we derive an analytical expression for the evolution of the mean postseismic cumulative displacement on an asperity surrounded by stable creep in response to a coseismic Coulomb stress step Δcff. The system is characterized by a density of asperities ρ defined as the ratio between velocity weakening ($(a-b)_w < 0$) and velocity strengthening areas ($(a-b)_s > 0$) on the fault. After the stress step, aftershocks will occur on the asperity and we define t_n as the timing of earthquake n. Furthermore, we call T_n the time delay between earthquake n and $n+1$, and we define a nondimensional parameter y that corresponds to the percentage of one seismic cycle. Thus, y is given by

$$y = \frac{t - t_n}{T_n}, \tag{B1}$$

where t is the time after the stress perturbation. In order to simplify the notations used in the following developments, we will write the quantities averaged in time over the seismic cycle n with an overbar and a subscript n and the quantities averaged in space over the entire fault plane with the average symbol. For instance, the different average values of the function $f(\mathbf{x}, t)$ that depend on both position $\mathbf{x}$ along the fault and time t will be defined by

$$\bar{f}_n = \frac{1}{T_n}\int_{t_n}^{t_{n+1}} f(\mathbf{x}, t)\mathrm{d}t,$$

$$\langle f \rangle = \frac{1}{S}\int_S f(\mathbf{x}, t)\mathrm{d}\mathbf{x},$$

where S denotes the area of the fault.

[54] In the following, we will consider that the entire fault segment behaves like a spring-block system forced at a constant rate v_p and undergoing rate-and-state friction. On each point of the fault, the frictional strength $\tau(\mathbf{x}, t)$ depends on the sliding velocity v and the state variable Θ as given by the rate-and-state friction law (1). The evolution of v and Θ after a positive stress perturbation are represented in Figures B1a and B1d, respectively. As suggested by the trajectories of the system in the phase diagrams of Figures 3 and 4, the relaxation of v and Θ is also presented in a rescaled way in Figures B1b, B1c, B1e, and B1f, and from these latter plots, it appears that their evolution is well described by a single periodic function (ν or θ) that is modulated by a slow varying function that relaxes toward a constant shape, leading to the Omori law for the number of aftershocks on the asperity. In order to separate the long-term evolution of the mean level from the periodic component, we will use the normalization presented in Figure B1 by assuming a sliding velocity and a state variable of the form:

$$\begin{cases} v(\mathbf{x}, t) &= \bar{v}_n \nu(\mathbf{x}, y) \\ \Theta(\mathbf{x}, t) &= \bar{\Theta}_n(\mathbf{x}) + \theta(\mathbf{x}, y). \end{cases} \tag{B2}$$

Here we consider that $\bar{v}_n$ and $\bar{\Theta}_n$ are constant between t_n and t_{n+1}, but evolve from one cycle to another and thus depend on n. Furthermore, $\bar{v}_n$ does not depend on $\mathbf{x}$, because otherwise the fault would accumulate stress from one cycle to another. The spatial variability and the temporal evolution at the timescale of the seismic cycle n are taken into account by the periodic functions ν and θ which correspond to the functions plotted in Figure B1. From the definition of $\bar{v}_n$ and $\bar{\Theta}_n$, we have

$$\bar{\nu} = 1, \bar{\theta} = 0.$$

Reinjecting (B2) into the expression (1) of the rate-and-state frictional strength and averaging the result over the seismic cycle n, we get

$$\bar{\tau}_n(\mathbf{x}) = \mu_0\sigma_1 + a(\mathbf{x})\sigma_1 \ln\frac{\bar{v}_n}{v_p} + a(\mathbf{x})\sigma_1 C_0(\mathbf{x}) + b(\mathbf{x})\sigma_1\bar{\Theta}_n(\mathbf{x}),$$

where σ_1 is the normal stress right after the perturbation, and C_0 is a constant given by

$$C_0(\mathbf{x}) = \overline{\ln \nu}_n = \int_0^1 \ln[\nu(\mathbf{x}, y)]\mathrm{d}y,$$

[55] Similarly, making use of (B2) into the state evolution law (2) between t_n and t_{n+1}, and assuming constant normal stress leads to

$$\dot{\Theta} = \frac{1}{T_n}\dot{\theta} = -\frac{\bar{v}_n \nu}{d_c}\left[\bar{\Theta}_n(\mathbf{x}) + \theta + \ln\frac{\bar{v}_n}{v_p} + \ln\nu\right].$$

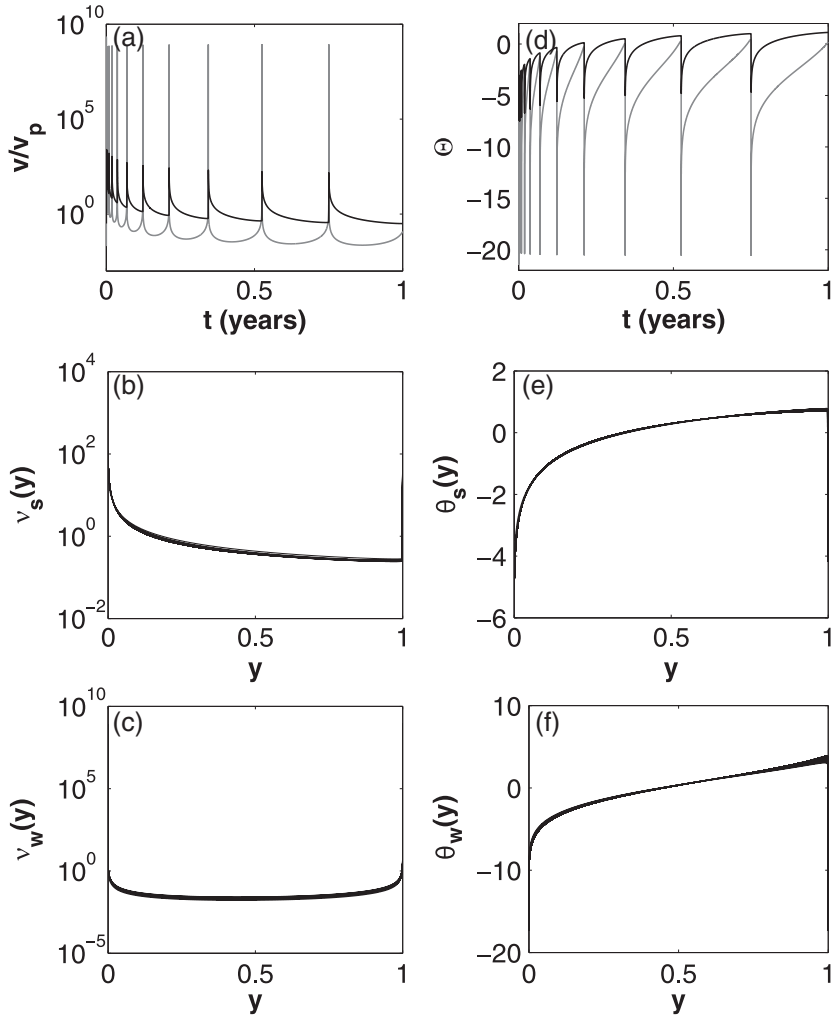

Figure B1. Sliding velocity v and state variable Θ after a positive Coulomb stress perturbation. (a) Velocity as a function of time t since the stress perturbation at the center of the asperity (gray) and on the antiasperity (black). (b) Normalized sliding velocity $\nu_w = v/\bar{v}_n$ at the center of the asperity, where $\bar{v}_n$ is the mean velocity during seismic cycle n as a function of percentage y of seismic cycle n. (c) Normalized sliding velocity ν_s on a point of the antiasperity. The normalization is the same as in Figure B1b. (d) State variable as a function of time since the stress perturbation. The colors have the same meaning than in Figure B1a. (e) Difference between state variable and mean value of the state variable $\bar{\Theta}_n$ during seismic cycle n $\left(\theta_w = \Theta - \bar{\Theta}_n\right)$ as a function of percentage y of seismic cycle n, at the center of the asperity. (f) Same diagram as Figure B1e but for a point on the antiasperity, as indicated by the subscript s in θ_s. These results are obtained for a density of asperities $\rho = 0.3$, and a stress perturbation $\Delta cff = 0.8$ MPa.

Furthermore, since θ is periodic, the mean value of $\dot{\theta}$ over a cycle vanishes and we get, after averaging,

$$\bar{\Theta}_n(\mathbf{x}) = -\ln\frac{\bar{v}_n}{v_p} - C_1(\mathbf{x}) - C_2(\mathbf{x}), \tag{B3}$$

where C_1 and C_2 are given by

$$C_1(\mathbf{x}) = \int_0^1 \nu(\mathbf{x},y)\ln[\nu(\mathbf{x},y)]\mathrm{d}y,$$

$$C_2(\mathbf{x}) = \int_0^1 \nu(\mathbf{x},y)\theta(\mathbf{x},y)\mathrm{d}y.$$

Note that expression (B3) also holds for the aging law. Making use of the separable solution (B2) indeed leads to

$$\dot{\Theta} = \frac{1}{T_n}\dot{\theta} = \frac{v_p}{d_c}e^{-\bar{\Theta}_n-\theta} - \frac{\bar{v}_n}{d_c}v.$$

After simplification and averaging, this latter expression becomes

$$\bar{\Theta}_n(\mathbf{x}) = -\ln\frac{\bar{v}_n}{v_p} + \ln D(\mathbf{x}) \tag{B4}$$

where $D(\mathbf{x})$ is given by

$$D(\mathbf{x}) = \int_0^1 e^{-\theta(\mathbf{x},y)}\mathrm{d}y.$$

Finally, we end up with the following expression of $\bar{\tau}_n$ in the case of the slip law:

$$\bar{\tau}_n(\mathbf{x}) = \mu_0\sigma_1 + [a(\mathbf{x}) - b(\mathbf{x})]\sigma_1 \ln\frac{\bar{v}_n}{v_p} + \sigma_1 C(\mathbf{x}), \tag{B5}$$

where C is defined by

$$C(\mathbf{x}) = a(\mathbf{x})C_0(\mathbf{x}) - b(\mathbf{x})\left[C_1(\mathbf{x}) + C_2(\mathbf{x})\right].$$

The most important point highlighted by equation (B5) is that the mean stress $\bar{\tau}_n$ is equal to the steady state frictional stress when the system slips at $\bar{v}_n$, and it is heterogeneous on the fault only if the friction parameter $(a-b)$ and the constant C are heterogeneous. The frictional strength $\langle\bar{\tau}_n\rangle$ averaged over the fault plane is given by

$$\langle\bar{\tau}_n\rangle = \mu_0\sigma_1 + A\sigma_1 \ln\frac{\bar{v}_n}{v_p} + \sigma_1\langle C(\mathbf{x})\rangle. \tag{B6}$$

where A is an effective friction coefficient defined as the average value of $(a-b)$ over the entire fault plane, so that

$$A = \langle[a(\mathbf{x}) - b(\mathbf{x})]\rangle = \rho(a-b)_w + (1-\rho)(a-b)_s. \tag{B7}$$

[56] We have derived the spatially averaged frictional strength of the equivalent spring and slider system characterizing the fault with a density of asperities ρ. In order to obtain an expression for the evolution of the mean displacement over the fault, we will equate this frictional stress to the average quasi-static elastic stress $\langle\bar{\tau}_n^e\rangle$. For that we will derive successively two expressions of $\langle\bar{\tau}_n^e\rangle$: first in the case of an infinite fault plane that corresponds to the periodic geometry used in our simulations, then in the more realistic case of a finite fault where slip vanishes at a distance $L/2$ from the center of the asperity.

B1. Mean Displacement on a Periodic Fault Plane

[57] From equation (5) for a constant and uniform $\Delta\tau$ and after neglecting the damping term, we have

$$\bar{\tau}_n^e(\mathbf{x}) = \mu_0\sigma - \frac{G}{w}\left[\bar{\delta}_n - \bar{\delta}_n^l\right] + \left[\bar{\delta}_n - \bar{\delta}_n^l\right]\int_S \kappa(\mathbf{x}-\mathbf{x_0})\mathrm{d}\mathbf{x_0} + \Delta\tau,$$

where δ and δ^l are, respectively, the cumulative displacement on the fault S and the loading displacement imposed at a distance $w/2$ in the fault-normal direction, and $\Delta\tau$ is the amplitude of the constant and uniform shear stress perturbation step. We also assumed that $\tau^* = \mu_0\sigma$, which is necessary to have a balance between elastic and frictional strength when the fault is sliding at the steady velocity v_p before any perturbation. Furthermore, since $\bar{\delta}_n$ and $\bar{\delta}_n^l$ are independent of $\mathbf{x_0}$, they have been taken out from the elastic interactions term in equation (5). Noting that κ is a periodic kernel, its integral over the fault vanishes (homogeneous unit slip on an infinite planar fault does not produce any stress) so that

$$\int_S \kappa(\mathbf{x}-\mathbf{x_0})\mathrm{d}\mathbf{x_0} = 0. \tag{B8}$$

After using this latter simplification and an averaging over the entire fault, we end up with the following expression of $\langle\bar{\tau}_n^e\rangle$:

$$\langle\bar{\tau}_n^e\rangle = \mu_0\sigma - \frac{G}{w}\left[\langle\bar{\delta}_n\rangle - \langle\bar{\delta}_n^l\rangle\right] + \Delta\tau, \tag{B9}$$

[58] The quasi-static equilibrium of the equivalent spring and slider system $\left(\langle\bar{\tau}_n^e\rangle = \langle\bar{\tau}_n\rangle\right)$ finally leads to the following equation:

$$A\sigma_1 \ln\frac{\bar{v}_n}{v_p} + \langle C(\mathbf{x})\rangle\sigma_1 = -k\left(\bar{\delta}_n - \bar{\delta}_n^l\right) + \Delta cff,$$

where $k = G/w$, and after assuming $\langle\bar{v}_n\rangle = \bar{v}_n$, $\langle\bar{\delta}_n\rangle = \bar{\delta}_n$, and $\langle\bar{\delta}_n^l\rangle = \bar{\delta}_n^l$ since $\bar{v}_n$, $\bar{\delta}_n$, and $\bar{\delta}_n^l$ do not depend on $\mathbf{x}$. Before the onset of any stress perturbation, the mean displacement during one seismic cycle is equal to the mean displacement of the loading point, so that the quasi-static equilibrium leads to $\langle C(\mathbf{x})\rangle = 0$. This latter property indicates that the average frictional stress is at steady state, which was already outlined by the crosses the phase diagrams of Figures 3 and 4. Thus, we end up with

$$A\sigma_1 \ln\frac{\bar{v}_n}{v_p} = -k\left(\bar{\delta}_n - \bar{\delta}_n^l\right) + \Delta cff. \tag{B10}$$

In the following, we will use $\bar{v}(t)$ and $\bar{\delta}(t)$ instead of $\bar{v}_n$ and $\bar{\delta}_n$, and we will replace $\bar{\delta}_n^l$ by $v_p t$. The solution of equation (B10) is simply

$$\bar{\delta}(t) = v_p t_r \ln\left[1 + e^{\Delta cff/A\sigma_1}\left(e^{t/t_r} - 1\right)\right], \tag{B11}$$

where t_r is a characteristic timescale that characterizes the relaxation of the mean cumulative displacement on the fault and thus the duration of the aftershock sequence on the asperity. It appears that this duration depends on the effective friction parameter A in the following way:

$$t_r = \frac{A\sigma_1}{kv_p}. \tag{B12}$$

For $t \gg t_r$, the mean cumulative displacement reaches the asymptotic regime $\bar{\delta}_\infty$ defined by:

$$\bar{\delta}_\infty(t) = v_p t + \frac{\Delta cff}{k} \tag{B13}$$

B2. Mean Displacement on a Finite Fault Plane

[59] Instead of considering an infinite repetition of the creep and asperity system of Figure 1, we focus on the particular situation of a single portion of fault composed of an asperity and its creeping environment, with vanishing slip on the remaining fault plane. We will denote by S the area occupied by the asperity and its creeping surroundings, and $\bar{S}$ the area of the fault where $\delta = 0$. In these conditions, equation (5) could be written as

$$\begin{aligned}\tau_e(\mathbf{x},t) = \tau^* &- \frac{G}{w}\left[\delta(\mathbf{x},t) - v_p t\right] \\ &+ \int_S \kappa_{np}(\mathbf{x}-\mathbf{x_0})\left[\delta(\mathbf{x_0},t) - v_p t\right]\mathrm{d}\mathbf{x_0} \\ &- v_p t\int_{\bar{S}} \kappa_{np}(\mathbf{x}-\mathbf{x_0})d\mathbf{x_0} \\ &- \eta\left[v(\mathbf{x},t) - v_p\right] + \Delta\tau(\mathbf{x},t),\end{aligned} \tag{B14}$$

where $\kappa_{np}(\mathbf{x}-\mathbf{x_0})$ is the shear stress on $\mathbf{x}$ associated with motion on $\mathbf{x_0}$. κ_{np} defers from κ in the sense that it is not periodic. The fourth term on the right-hand side of (B14) corresponds to the boundary effect. Note that we still have the following condition on κ_{np}:

$$\int_{S+\bar{S}} \kappa_{np}(\mathbf{x}-\mathbf{x_0})\mathrm{d}\mathbf{x_0} = 0,$$

so that equation (B14) reduces to

$$\begin{aligned}\tau_e(\mathbf{x},t) = \tau^* &- \frac{G}{w}\left[\delta(\mathbf{x},t) - v_p t\right] \\ &+ \int_S \kappa_{np}(\mathbf{x}-\mathbf{x_0})\delta(\mathbf{x_0},t)\mathrm{d}\mathbf{x_0} \\ &- \eta\left[v(\mathbf{x},t) - v_p\right] + \Delta\tau(\mathbf{x},t).\end{aligned} \tag{B15}$$

Averaging equation (B15) in time and over S leads to, after neglecting the radiation damping term:

$$\left\langle \bar{\tau}_n^e \right\rangle = \mu_0\sigma - \frac{G}{w}\left[\left\langle \bar{\delta}_n \right\rangle - \left\langle \bar{\delta}_n^l \right\rangle\right] - \Delta\tau_S + \Delta\tau,$$

where $\Delta\tau_S$ is the mean stress drop associated with mean slip $\left\langle \bar{\delta}_n \right\rangle$ on the fault S. Assuming that S is circular of radius R_0 and that the displacement profile $\bar{\delta}_n(\mathbf{x_0})$ on S is elliptical, the circular crack solution of *Eshelby* [1957] leads to the following expression for $\Delta\tau_S$:

$$\Delta\tau_S = k_l\left\langle \bar{\delta}_n \right\rangle = \frac{7\pi G}{24R_0}\left\langle \bar{\delta}_n \right\rangle,$$

where $k_l = 7\pi G/24R_0$ is the equivalent stiffness associated with the interaction with the locked boundary.

[60] The quasi-static equilibrium of the equivalent spring and slider system is here given by

$$A\sigma_1 \ln\frac{\bar{v}_n}{v_p} + \left\langle C(\mathbf{x}) \right\rangle \sigma_1 = -k\left(\bar{\delta}_n - \bar{\delta}_n^l\right) - k_l\bar{\delta}_n + \Delta cff, \tag{B16}$$

which leads to the following expression of the mean cumulative displacement on the fault:

$$\bar{\delta}(t) = v_l t_r \ln\left[1 + e^{\Delta cff_l/A\sigma_1(1+kl/k)}\left(e^{t/t_r} - 1\right)\right], \tag{B17}$$

where t_r is the characteristic defined by (B12), $\Delta cff_l = \Delta cff - \left\langle C(\mathbf{x}) \right\rangle \sigma_1$, and v_l is a characteristic velocity given by

$$v_l = \frac{k}{k+k_l}v_p, \tag{B18}$$

which reduces to v_p when $k_l = 0$. For $t \gg t_r$, the asymptotic behavior of the cumulative displacement becomes

$$\bar{\delta}_\infty(t) = v_l t + v_l t_r\left[\ln\left(1 + \frac{k_l}{k}\right) + \frac{\Delta cff_l}{A\sigma_1}\right]. \tag{B19}$$

Appendix C: Creep Amplification of Tectonic Stress on the Asperity

[61] The derivation of a seismicity rate from the cumulative displacement formula (12) after a stress perturbation requires the estimation of the total stressing rate acting on the asperity. As mentioned in the main text, the asperity is forced both by a tectonic loading at v_p through stiffness $k = G/w$, where G is the shear modulus of the elastic medium and w its thickness, and by the accelerated slip on the antiasperity region through equivalent stiffness k_a. Here we propose an estimation of the magnitude of k_a. For that, we will use the Green function of *Maruyama* [1964] relating stress at some point of the fault to unit slip at another point. In order to estimate k_a, we will assimilate it with the stress generated at the center of a circular asperity of radius R surrounded by an annulus of largest dimension equal to $L/2$, the half length of the fault, and experiencing a uniform unit slip while the asperity remains locked. According to *Maruyama* [1964], the stress generated at the center of the asperity k_a is given by

$$k_a = \int_R^{L/2}\int_0^{2\pi} \frac{G}{4\pi}\left[\frac{2(1-\alpha_0)}{r^3} - 3(1-2\alpha_0)\frac{\cos^2\phi}{r^3}\right] r\mathrm{d}r\mathrm{d}\phi, \tag{C1}$$

where $\alpha_0 = (\lambda + G)/(\lambda + 2G)$, λ and G being the Lame parameters. We end up with

$$k_a = \frac{G}{4}(1+2\alpha_0)\left[\frac{1}{R} - \frac{2}{L}\right]. \tag{C2}$$

[62] Assuming $R \ll L/2$ and $R \ll w$, the ratio between k_a and k becomes

$$\frac{k}{k_a} = \frac{4R}{(1+2\alpha_0)w} \ll 1. \tag{C3}$$

Note that the assumption $R \ll L$ is more relevant in the periodic geometry we use for the numerical simulations than for a real fault. In our simulations, the creeping part of the fault plane is indeed of infinite dimension so that $2/L$ vanishes, and the expression (C2) gives the approximate stiffness if the effect of the images of the asperity is neglected. On the other hand, on a real fault, the creeping segments are of finite dimension so that the $2/L$ term is larger than in the numerical model.

[63] **Acknowledgments.** This work benefited from the support of the École Normale Supérieure (ENS) grant, the seismological laboratory of the Institut de Physique du Globe de Paris (IPGP), and the ANR project ASEISMIC. It is also integrated in the European program REAKT.

References

Ader, T. J., J.-P. Ampuero, and J.-P. Avouac (2012), The role of velocity-neutral creep on the modulation of tectonic tremor activity by periodic loading, *Geophys. Res. Lett.*, *39*, L16310, doi:10.1029/2012GL052326.

Ampuero, J., and A. Rubin (2008a), Earthquake nucleation on rate and state faults: Aging and slip laws, *J. Geophys. Res.*, *113*, B01302, doi:10.1029/2007JB005082.

Ampuero, J., and A. Rubin (2008b), Earthquake nucleation on rate and state faults: Aging and slip laws, *J. Geophys. Res.*, *113*, B01302, doi:10.1029/2007JB005082.

Ariyoshi, K., T. Hori, J.-P. Ampuero, Y. Kaneda, T. Matsuzawa, R. Hino, and A. Hasegawa (2009), Influence of interaction between small asperities on various types of slow earthquakes in a 3-D simulation for a subduction plate boundary, *Gondwana Res.*, *16*(3), 534–544.

Ariyoshi, K., T. Matsuzawa, J. Ampuero, R. Nakata, T. Hori, Y. Kaneda, R. Hino, and A. Hasegawa (2012), Migration process of very low-frequency events based on a chain-reaction model and its application to the detection of preseismic slip for megathrust earthquakes, *Earth Planets Space*, *64*(8), 693–702.

Belardinelli, M., A. Bizzarri, and M. Cocco (2003), Earthquake triggering by static and dynamic stress changes, *J. Geophys. Res.*, *108*(B3), 2135, doi:10.1029/2002JB001779.

Blanpied, M., C. Marone, D. Lockner, J. Byerlee, and D. King (1998), Quantitative measure of the variation in fault rheology due to fluid-rock interactions, *J. Geophys. Res.*, *103*(B5), 9691–9712.

Bourouis, S., and P. Bernard (2007), Evidence for coupled seismic and aseismic fault slip during water injection in the geothermal site of Soultz (France), and implications for seismogenic transients, *Geophys. J. Int.*, *169*(2), 723–732, doi:10.1111/j.1365-246X.2006.03325.x.

Chen, T., and N. Lapusta (2009), Scaling of small repeating earthquakes explained by interaction of seismic and aseismic slip in a rate and state fault model, *J. Geophys. Res.*, *114*, B01311, doi:10.1029/2008JB005749.

Dieterich, J. (1994), A constitutive law for rate of earthquake production and its application to earthquake clustering, *J. Geophys. Res.*, *99*(B2), 2601–2618.

Dieterich, J. H. (1979), Modeling of rock friction-1. Experimental results and constitutive equations, *J. Geophys. Res.*, *84*(B5), 2161–2168.

Dreger, D., R. Nadeau, and A. Chung (2007), Repeating earthquake finite source models: Strong asperities revealed on the San Andreas Fault, *Geophys. Res. Lett.*, *34*, L23302, doi:10.1029/2007GL031353.

Dublanchet, P., P. Bernard, and P. Favreau (2013), Interaction and triggering in a 3D rate-and-state asperity model, *J. Geophys. Res. Solid Earth*, *118*, 2225–2245, doi:10.1002/jgrb.50187.

Eshelby, J. (1957), The determination of the elastic field of an ellipsoidal inclusion, and related problems, *Proc. R. Soc. London, Ser. A. Math. Phys. Sci.*, *241*(1226), 376–396.

Gomberg, J., N. Beeler, M. Blanpied, and P. Bodin (1998), Earthquake triggering by transient and static deformations, *J. Geophys. Res.*, *103*(B10), 24,411–24,426.

Gomberg, J., N. Beeler, and M. Blanpied (2000), On rate-state and Coulomb failure models, *J. Geophys. Res*, *105*(14), 7857–7872.

Gomberg, J., P. Reasenberg, M. Cocco, and M. Belardinelli (2005), A frictional population model of seismicity rate change, *J. Geophys. Res.*, *110*, B05S03, doi:10.1029/2004JB003404.

Harris, R. A. (1998), Introduction to special section: Stress triggers, stress shadows, and implications for seismic hazard, *J. Geophys. Res.*, *103*(B10), 24,347–24,358.

Harris, R., and R. Simpson (1998), Suppression of large earthquakes by stress shadows: A comparison of Coulomb and rate-and-state failure, *J. Geophys. Res.*, *103*(B10), 24,439–24,451.

Helmstetter, A., and B. Shaw (2009), Afterslip and aftershocks in the rate-and-state friction law, *J. Geophys. Res.*, *114*, B01308, doi:10.1029/2007JB005077.

Kaneko, Y., and N. Lapusta (2008), Variability of earthquake nucleation in continuum models of rate-and-state faults and implications for aftershock rates, *J. Geophys. Res.*, *113*, B12312, doi:10.1029/2007JB005154.

Kaneko, Y., J. Avouac, and N. Lapusta (2010), Towards inferring earthquake patterns from geodetic observations of interseismic coupling, *Nat. Geosci.*, *3*(5), 363–369.

Kato, N. (2003), Repeating slip events at a circular asperity: Numerical simulation with a rate-and state-dependent friction law, *Bull. Earthq. Res. Inst.*, *78*, 151–166.

Kato, N. (2004), Interaction of slip on asperities: Numerical simulation of seismic cycles on a two-dimensional planar fault with nonuniform frictional property, *J. Geophys. Res.*, *109*, B12306, doi:10.1029/2004JB003001.

Kato, N. (2007), Expansion of aftershock areas caused by propagating postseismic sliding, *Geophys. J. Int.*, *168*(2), 797–808.

Kilgore, B. D., M. L. Blanpied, and J. H. Dieterich (1993), Velocity dependent friction of granite over a wide range of conditions, *Geophys. Res. Lett.*, *20*(10), 903–906.

King, G., R. Stein, and J. Lin (1994), Static stress changes and the triggering of earthquakes, *Bull. Seismol. Soc. Am.*, *84*(3), 935–953.

Lengliné, O., et al. (2009), Inferring the coseismic and postseismic stress changes caused by the 2004 M_W = 6 Parkfield earthquake from variations of recurrence times of microearthquakes, *J. Geophys. Res.*, *114*, B10303, doi:10.1029/2008JB006118.

Linker, M. F., and J. H. Dieterich (1992), Effects of variable normal stress on rock friction: Observations and constitutive equations, *J. Geophys. Res.*, *97*(B4), 4923–4940.

Marone, C. (1998), Laboratory-derived friction laws and their application to seismic faulting, *Annu. Rev. Earth Planet. Sci.*, *26*(1), 643–696.

Marone, C. J., C. Scholtz, and R. Bilham (1991), On the mechanics of earthquake afterslip, *J. Geophys. Res.*, *96*(B5), 8441–8452.

Maruyama, T. (1964), 16. statical elastic dislocations in an infinite and semi-infinite medium, *Bull. Earthq. Res. Inst.*, *42*, 289–368.

Murray, J., P. Segall, P. Cervelli, W. Prescott, and J. Svarc (2001), Inversion of GPS data for spatially variable slip-rate on the San Andreas Fault near Parkfield, CA, *Geophys. Res. Lett*, *28*(2), 359–362.

Nadeau, R., and L. Johnson (1998), Seismological studies at Parkfield VI: Moment release rates and estimates of source parameters for small repeating earthquakes, *Bull. Seismol. Soc. Am.*, *88*(3), 790–814.

Omori, F. (1894), On after-shocks.

Perfettini, H., and J. Ampuero (2008), Dynamics of a velocity strengthening fault region: Implications for slow earthquakes and postseismic slip, *J. Geophys. Res.*, *113*, B09411, doi:10.1029/2007JB005398.

Perfettini, H., and J. Avouac (2004), Postseismic relaxation driven by brittle creep: A possible mechanism to reconcile geodetic measurements and the decay rate of aftershocks, application to the Chi-Chi earthquake, Taiwan, *J. Geophys. Res*, *109*, B02304, doi:10.1029/2003JB002488.

Perfettini, H., J. Schmittbuhl, and A. Cochard (2003), Shear and normal load perturbations on a two-dimensional continuous fault: 1. Static triggering, *J. Geophys. Res.*, *108*(B9), 2408, doi:10.1029/2002JB001804.

Press, W. H., S. A. Teukolsky, W. T. Vetterling, and B. P. Flannery (2007), *Numerical Recipes Source Code CD-ROM 3rd Edition: The Art of Scientific Computing* 3rd ed., Cambridge University Press, New York, NY, USA.

Rice, J. (1992), Fault stress states, pore pressure distributions, and the weakness of the San Andreas Fault, *Int. Geophys. Ser.*, *51*, 475–475.

Rice, J. R. (1983), Constitutive relations for fault slip and earthquake instabilities, *Pure Appl. Geophys.*, *121*(3), 443–475.

Rice, J. R. (1993), Spatiotemporal complexity of slip on a fault, *J. Geophys. Res.*, *98*(B6), 9885–9907.

Rubin, A., and J. Ampuero (2005), Earthquake nucleation on (aging) rate and state faults, *J. Geophys. Res.*, *110*, B11312, doi:10.1029/2005JB003686.

Ruina, A. L. (1983), Slip instability and state variable friction laws, *J. Geophys. Res.*, *88*(B12), 10,359–10,370.

Schaff, D., G. Beroza, and B. Shaw (1998), Postseismic response of repeating aftershocks, *Geophys. Res. Lett*, *25*(24), 4549–4552.

Skarbek, R., A. Rempel, and D. Schmidt (2012), Geologic heterogeneity can produce aseismic slip transients, *Geophys. Res. Lett.*, *39*, L21306, doi:10.1029/2012GL053762.

Stein, R. (1999), The role of stress transfer in earthquake occurrence, *Nature*, *402*(6762), 605–609.

Stein, R., A. Barka, and J. Dieterich (2007), Progressive failure on the North Anatolian Fault since 1939 by earthquake stress triggering, *Geophys. J. Int.*, *128*(3), 594–604, doi:10.1038/45144.

Swarztrauber, P. (1982), Vectorizing the fast Fourier transforms, in *Parallel Computations*, edited by Garry Rodrigue, pp. 51–83, Academic Press, New York.

Swarztrauber, P. (1984), FFT algorithms for vector computers, *Parallel Comput.*, *1*(1), 45–63.

Titus, S., C. DeMets, and B. Tikoff (2006), Thirty-five-year creep rates for the creeping segment of the San Andreas Fault and the effects of the 2004 Parkfield earthquake: Constraints from alignment arrays, continuous global positioning system, and creep meters, *Bull. Seismol. Soc. Am.*, *96*(4B), S250–S268.

Toda, S., R. Stein, P. Reasenberg, J. Dieterich, and A. Yoshida (1998), Stress transferred by the 1995 $M(W)$ = 6.9 Kobe, Japan, shock–Effect on aftershocks and future earthquake probabilities, *J. Geophys. Res.*, *103*(B10), 24,543–24,565.

Toda, S., R. Stein, K. Richards-Dinger, and S. Bozkurt (2005), Forecasting the evolution of seismicity in Southern California: Animations built on earthquake stress transfer, *J. Geophys. Res.*, *110*, B05S16, doi:10.1029/2004JB003415.

Tse, S., and J. Rice (1986), Crustal earthquake instability in relation to the depth variation of frictional slip properties, *J. Geophys. Res.*, *91*(B9), 9452–9472.

Utsu, T., Y. Ogata, and R. Matsu'ura (1995), The centenary of the Omori formula for a decay law of aftershock activity, *J. Phys. Earth*, *43*(1), 1–33.

Vidale, J., W. Ellsworth, A. Cole, and C. Marone (1994), Variations in rupture process with recurrence interval in a repeated small earthquake, *Nature*, *368*(6472), 624–626.

Ziv, A. (2007), On the nucleation of creep and the interaction between creep and seismic slip on rate-and state-dependent faults, *Geophys. Res. Lett.*, *34*, L15303, doi:10.1029/2007GL030337.